Universidad de Concepción
Dirección de Postgrado
Facultad de Ciencias Físicas y Matemáticas – Programa de Magíster en Ciencias con Mención en Física

Modelos de Energía Oscura y Contraste Observacional

Tesis para optar al grado académico de
Magíster en Ciencias con Mención en Física

Jorge Johnny Moya Abuhadba

Concepción, Chile
Enero, 2017

Profesores Guía: Fabiola Arévalo
Antonella Cid
Guillermo Rubilar

Contents

List of Figures **iv**

List of Tables **vi**

Resumen **vii**

Abstract **ix**

Agradecimientos **xi**

1 Introduction **1**

2 Elements of Cosmology **3**
2.1 Relativistic Cosmology . . . 3
2.1.1 Dynamics of Friedmann-Lemaître-Robertson-Walker spacetime . . . 4
2.2 Lambda Cold Dark Matter model . . . 6
2.3 Alternative models . . . 8
2.3.1 Omega Cold Dark Matter model . . . 8
2.3.2 Dark Energy Parametrizations . . . 8
2.3.3 Quintessence model . . . 9
2.4 Cosmological Interaction . . . 9
2.5 Observational Cosmology . . . 11
2.5.1 Distance indicators . . . 13
2.5.2 Apparent Magnitude . . . 15
2.5.3 Hubble function . . . 17
2.5.4 Baryonic Acoustic Oscillations . . . 17
2.5.5 Cosmic Microwave Background . . . 18

3 Data Fitting and Model Comparison **21**
3.1 Maximum Likelihood . . . 21
3.2 Method of Least Squares . . . 22
3.3 Bayesian Analysis . . . 23
3.3.1 Akaike Information Criteria . . . 25
3.3.2 Bayesian Information Criteria . . . 25

4 Analysis and Results **27**
4.1 Theoretical Interactions . . . 27
4.2 Observational analysis . . . 28
4.3 Model fitting . . . 30

5 Conclusion **39**

A Elements of data fitting **41**
A.1 Chi-Square Distribution 41
A.2 Confidence Limits on Estimated Model Parameters 42
A.3 Probability Distribution in the Normal Case 42
A.3.1 Example 3: Maximum Likelihood 47
A.4 Propagation of uncertainties 47
A.5 Minimization Algorithm 48

Bibliography **51**

List of Figures

2.1 Examples of constant curvature 2D surfaces. 5
2.2 Graphics of the evolution of the normalized energy densities, matter ($\Omega_{\rm m}$), radiation ($\Omega_{\rm r}$) and cosmological constant (Ω_Λ). 7
2.3 Scheme of the Universe's expansion. 12
2.4 CMB spectrum. 12
2.5 Scheme where P point sends light rays to the point O. 14
2.6 Planck 2015 temperature power spectrum. 20

3.1 Illustration of a physical phenomenon observed. 24
3.2 At left Hypothesis of one box and at right Hypotesis of two boxes. 24

4.1 ΔAIC and ΔBIC of models defined in Table 4.1 compared to ΛCDM. 32
4.2 Models defined in Table 4.1 compared to the ωCDM model. 32
4.3 Coincidence parameter in semilog scale. 33
4.4 Semilog graphic of the evolution of the density parameters for the interacting model Γ_{8a} considering Union 2.1 $+H(z)$+BAO 33
4.5 Deceleration parameter considering data from Union 2.1, $H(z)$ and BAO. 35
4.6 Effective parameter of state $\omega_{\rm eff}$ considering data from Union 2.1, $H(z)$ and BAO. 36

A.1 Chi-square distribution for different values of ν. 41
A.2 χ^2 distribution for $\nu = 1$ (left) and $\nu = 2$ (right). 43
A.3 Straight line example. 44
A.4 These are the contours of our example. 44
A.5 Combined histograms of synthetic data. 45
A.6 Chi-square distribution of the example. 46
A.7 Histograms of δa_0 and δa_1. 46
A.8 Histogram of $\Delta\chi^2$. 46
A.9 Histogram of $\Delta\chi^2_\nu$, where a_0 was set and a_1 was fitted in each simulation. 47

List of Tables

2.1 Parameterizations, where ω_0 and ω_1 are constants. 9
2.2 Expressions for the constants b_1, b_2 and b_3 for the considered interaction. 11

4.1 Results of the data fitting using the joint analysis from Union 2.1, $H(z)$ and BAO. 31
4.2 Results of the data fitting using the joint analysis from Union 2.1 and $H(z)$. . . . 31
4.3 Ranking of models according to BIC. 32
4.4 Results of the data fitting using the joint analysis from Constitution, $H(z)$ and BAO. 34
4.5 Results of the data fitting using the joint analysis from Union 2, $H(z)$ and BAO. 34
4.6 Results of the data fitting using the joint analysis from Constitution and $H(z)$. . 37
4.7 Results of the data fitting using the joint analysis from Union 2 and $H(z)$. 37

A.1 $\Delta\chi^2$ as a function of confidence level p and number of parameters ν. 43

Resumen

En esta tesis estudiamos escenarios alternativos al modelo Lambda Cold Dark Matter para la evolución del Universo tardío. Usando la métrica de Friedmann-Lemaître-Robertson-Walker en el marco de la teoría de Relatividad General de Einstein, investigamos interacciones cosmológicas lineales y no lineales donde la materia oscura y la energía oscura interactúan, transfiriendo energía de una a otra. En particular, nos centramos en modelos de interacción que poseen solución analítica en función del factor de escala cosmológico. Con el fin de analizar cómo estos modelos ajustan los datos observacionales , usamos criterios desarrollados en teoría de información. En particular nos centramos en dos criterios: el critero de infomación de Akaike y el criterio de información Bayesiano. Estos criterios penalizan a los modelos según el número de parámetros libres que poseen y por cómo ajustan ajustan los datos, permitiéndonos compararlos entre ellos. Para este propósito usamos datos observacionales de: Diferentes compilaciones de Supernovas tipo Ia (Constitution, Union 2, Union 2.1 y JLA agrupado), la función de Hubble $H(z)$, oscilaciones acústicas de bariones. Comparamos los modelos de interacción entre ellos analizando si modelos más complejos (modelos con más parámetros) son preferidos por estos criterios. En nuestros análisis encontramos algunas interacciones viables que alivian el problema de la coincidencia. Además, en algunos de estos modelos la dirección de la transferencia de energía entre materia oscura y energía oscura cambia durante la evolución del Universo. Finalmente, concluimos que de acuerdo a los criterios de información, modelos de interacción con el mismo número de parámetros libres ajustan los datos usados de forma similar, independientemente de la naturaleza de la interacción.

Abstract

In this thesis we study alternative scenarios to the Lambda Cold Dark Matter model for the evolution of the late Universe. Using the Friedmann-Lemaître-Robertson-Walker metric within the frame of Einstein's General Relativity theory, we investigate linear and non-linear cosmological interactions where dark matter and dark energy interact, transferring energy from one fluid to another. In particular, we focus on interacting models which have analytical solutions in terms of the scale factor. In order to analyze how these models fit the data we use criteria developed in information theory, in particular we focus in two criteria: the Akaike information criterion and the Bayesian information criterion. These criteria rank models according to the number of free parameters that they have and how well they fit the observational data, allowing us to compare among competing models. For this purpose we use observational data from: type Ia Supernovae (Constitution, Union 2, Union 2.1 and binned JLA compilations), Hubble function $H(z)$ and baryonic acoustic oscillations. We compare the interacting models to each other analysing whether more complex interacting models (models with more parameters) are favored by these criteria. In our analysis we find some viable interactions that alleviate the coincidence problem. Furthermore, in some of these models the direction of the energy transfer between dark matter and dark energy changes during the evolution of the Universe. Finally, we conclude that according to information criteria, interacting models with the same number of free parameters adjust the available data equally well, independent of the nature of interaction.

Agradecimientos

Durante mi periodo de formación en la Universidad de Concepción he pasado por muchas experiencias que me han hecho crecer como persona y he tenido el agrado de conocer a mucha gente que me ha apoyado en el ámbito académico y personal. Personas que de no haberlas conocido probablemente no habría llegado tan lejos y por eso debo agradecerles todo lo que han hecho por mí.

Quiero partir agradeciendo a quienes pocas veces se les toma en cuenta, pero que siempre han estado cuando se les necesita, me refiero a los paradocentes de la facultad, específicamente a: Don Juan Carlos Burgos y Don Heraldo Manríquez que siempre tuvieron un buen trato con los alumnos, dispuestos a ayudarnos hasta en lo más mínimo. También agradezco a las secretarias Soledad Daroch y Marta Astudillo por siempre preocuparse por los alumnos y sus necesidades, sin ellas la universidad no hubiese sido lo mismo. No puedo olvidar agradecer a Don Victor Venegas, encargado del Centro de Apoyo Académico, CAA más conocido como "Sala de Estudio", por ser un gran jefe, persona y amigo que me perdonó la vida en incontables ocaciones y siempre me entregó su apoyo.

Agradezco a mis compañeras Nataly Nicole Ibarra y Perla Soledad Medina por los buenos momentos y discuciones sobre Física que me sirvieron mucho para aclarar ideas y conceptos, en especial a esta última por subirme el ánimo en mis momentos de debilidad con su simpatía y buen humor. También agradezco a Luis Concha por ser un buen amigo y compañero que aunque ahora está estudiando lejos, sigue en la memoria colectiva de la facultad y especialmente en la de sus amigos.

También agradezco a todos los profesores que me hicieron clases, por entregarme los conocimientos y herramientas para alcanzar la meta de ser un Físico, en especial le agradezco a Juan Crisóstomo por sus excelentes clases en los varios cursos que tomé con él. A Jaime Araneda por todas las veces que le fui a consultar (cosas de computación y alemán entre otras) y él siempre se dio el tiempo de responder mis inquietudes a pesar de tener su agenda totalmente colapsada.

A Fabiola Arévalo y a Antonella Cid por guiarme en la Tesis, tenerme mucha, pero mucha paciencia tanto en lo académico y como fuera de ello y además les agradezco especialmente por no dejar de creer en mí. Sin duda alguna, no puedo pasar por alto agradecer a Guillermo Francisco Rubilar Alegría ("Dr. Alegría") por ser mi sensei, gurú de la Física o más bien por dejarme ser su "Padawan", por todos los consejos de vida que me dio y todas las veces que me apoyó para que siguiese adelante en el sendero de la Física, por aguantarme todas las veces que fui a su oficina a preguntarle, por ser un gran docente y persona.

Agradezco a mi familia, a mi papá (Jorge Moya), mi mamá (Yolanda Abuhadba), mi hermano (Rafael Moya) y a mi perro (Rex), porque todo este tiempo me han brindado su apoyo incondicional y su afecto.

A mis amigos de toda la vida Gianfranco Brebi ("GG"), Stephanie Caro ("Stephy Love"), Enrique Cores ("Kike"), Sebastian Ruiz ("Bazz") por brindarme su amistad, que a pesar de la distancia y el tiempo, siempre permanece constante. Porque sin ellos no sería quien soy ahora, les doy las gracias por ser tan buenos amigos.

A las tantas personas que tuve el agrado de conocer en estos años. Entre ellos: Roberto Salazar, Sra. Fatima Ramirez, Valeria Olivares, Nelvy Choque, Felipe Portales, Patricio Muñoz, Vanessa Hasbún, José Barrientos, Aldo Delgado, Victor Cardenas, Myrna Sandoval, Josefa Vilches, Elizabeth Gutierrez, Joaquin Díaz de Valdés, Oscar Saez, Verónica Alvarado, Teresa

Baeza, Camila Muñoz, Benjamin Nicólas, Frau Hanna, Maximiliano Ujevic, Mauricio Cataldo, Pedro Labraña, Freddy Paiva y Anahí Gajardo.

No puedo dejar de agradecer al Departamento de Física y al Programa de Magíster en Ciencias Físicas, por el apoyo financiero que me brindaron para viajar a congresos en el extranjero.

He dejado para el final a alguien que ha sido muy importante en mi paso por la universidad. Quiero agradecer especialmente a Felipe Matus ("El Cochinote"), por todos los buenos y malos momentos que hemos pasados mientras nos formábamos como Físicos. Por el gran apoyo que me ha brindado en lo académico y personal, por los consejos (casi siempre muy malos consejos con frases gramaticalmente incorrectas y usando palabras que él inventó, pero el gesto es lo que cuenta), por su humor irreverente, por las discusiones de Física, por las maratónicas tardes de video juegos. Básicamente le agradezco por ser un gran amigo.

A todos ustedes ¡Muchas Gracias!

Chapter 1

Introduction

The Universe contains everything that exists, including space and time. Observing the Universe we can see that it has all types of structures on a vast range of scales; atomic nuclei, atoms, molecules, and so on to form more complex structures such as planets orbiting stars, stars collected into galaxies, galaxies gravitationally bounded into clusters, and even clusters of galaxies within larger superclusters.

Cosmology, from ancient Greek κόσμο (kósmos, "world") + λογία (logía, "science"), is the scientific study of the large scale properties of the Universe as a whole. It uses the scientific method to understand the origin, evolution and ultimate fate of the entire Universe. Like any field of science, cosmology involves the formulation of theories or hypotheses about the Universe which make specific predictions for phenomena that can be tested with observations. Depending on the outcome of the observations, the theories will need to be abandoned, revised or extended to be consistent with the data.

Since at cosmological scale the gravitational interaction is the predominant, to describe the Universe we need to use a gravitational theory. At present, the prevailing theory of gravitation is the Einstein's theory of General Relativity, which explains the gravitational attraction as the effect of the curvature of spacetime in the presence of matter and/or energy. The Einstein field equations are nonlinear and very difficult to solve. Einstein used approximation methods in working out initial predictions of the theory. But as early as 1916, the astrophysicist Karl Schwarzschild found the first non-trivial exact solution to the Einstein field equations, the Schwarzschild metric. This solution laid the groundwork for the description of the final stages of gravitational collapse, and the objects known today as black holes. In 1917, Einstein applied his theory to the Universe as a whole, initiating the field of relativistic cosmology. In line with contemporary thinking, he assumed a static Universe, adding a new parameter to his original field equations, the *cosmological constant*. However, in 1929, the work of Edwin Hubble among others had shown that the Universe is expanding. This is readily described by the expanding cosmological solutions found by Alexander Friedmann in 1922. Later in 1931, George Lemaître formulate the earliest version of the Big Bang scenario, in which our Universe has evolved from an extremely hot and dense earlier state.

In the last 100 years cosmology has advanced significantly, especially in the observational area, there have been many methods to study the evolution of the Universe, such as studying the radiation from type Ia supernovae, the Cosmic Microwave Background radiation (CMB, a remanent radiation from an early epoch of the Universe), baryonic acoustic oscillations (BAO) and so on. Furthermore, databases have grown exponentially over the years. Observatories and satellites (such as Hubble space telescope, WMAP, Planck, among others) dedicated to collect data have increased in number and accuracy of the data. Currently the prevailing theory about the origin and evolution of our Universe is the so-called Big Bang theory. Under Big Bang theory the simplest model, so called Lambda Cold Dark Matter (ΛCDM), is the current "standard model" of cosmology, this model gives account of the evolution of the Universe. ΛCDM model establishes that the energy density of the Universe is dominated now by a non-relativistic

fluid (dark matter) and a cosmological constant Λ (dark energy).

Despite of the observational success of the ΛCDM scenario, this model has theoretical problems such as the fine-tuning problem and the coincidence problem and there are some observational tensions recently reported with this model, present when we use independently high redshift and low redshift data to constrain parameters. Therefore it is necessary to study new models to alleviate these problems, in particular, given that the nature of dark energy and dark matter is unknown and they dominate the energy content of the Universe today, it is reasonable to consider more general scenarios where dark matter and dark energy are phenomenologically coupled. In this manner, models based on the interaction between dark matter and dark energy have been studied to describe the accelerated expansion. One of the first interacting models was proposed to alleviate the coincidence problem in an interacting-quintessence scenario, focusing in an asymptotic attractor behavior for the ratio of the energy densities for the dark components. Since then, many interacting models with numerical and analytical solutions have emerged, also interactions with change of sign. In this sense, the interacting models help us to understand the nature of the Universe.

To compare different models of a certain physical phenomenon in light of the data there are criteria, based on the Occam's razor ("among competing hypotheses, the one with the fewest assumptions should be selected"). These criteria measure the goodness of fitted models compared to a base model. Two widely used criteria are the Akaike Information Criterion (AIC) and the Bayesian Information Criterion (BIC).

In this work we analyze eight general types of interacting models with analytical solution using supernovae type Ia (Constitution, Union, Union 2.1 and JLA), H(z) and BAO data under the Akaike information criterion and the Bayesian information criterion. The main goal of our work is to investigate if complex interacting models are competitive in fitting the data and whether we could distinguish among them via a model comparison approach based on information criteria.

In Chapter 2 we present elements of General Relativity and we describe cosmology in the theoretical framework of General Relativity. In Chapter 3 we study how to contrast models with observational data and how to compare models through information criteria. In Chapter 4 we analyze different interacting models in light of the aforementioned data through observational contrast and information criteria. In Chapter 5 we discuss the results and present the conclusions.

Chapter 2

Elements of Cosmology

Cosmology is based in two hypothesis the *Cosmological principle*, which says that the distribution of matter in the Universe is homogeneous and isotropic when viewed at large enough scales (larger than 10^7pc[1]) and the *Weyl's postulate*, which stipulates that the world lines of cosmological particles should be everywhere orthogonal to a family of spatial hypersurfaces [1]. The Weyl's postulate allows us define a "general time" for the Universe called cosmological time.

2.1 Relativistic Cosmology

In General Relativity (G.R.) it is assumed that the metric $g_{\mu\nu}$ of the spacetime is *lorentzian*. This means that the line element

$$ds^2 = g_{\mu\nu}(x)\, dx^\mu dx^\nu, \qquad \mu,\nu = 0,1,2,3, \tag{2.1.1}$$

is not positive-defined, i.e., it can be, for the same event P, positive, negative or zero, depending on the value of dx^μ. From here on, the convention for the signature of the metric will be $(+,-,-,-)$.

As natural extension of Special Relativity, in General Relativity it is assumed that massive bodies, under a gravitational field, describe world lines that can be parameterized through the *proper time* τ, defined as $ds = c\, d\tau$. Considering that $x^\mu(\lambda)$ is the world line of a massive body, then

$$\boxed{d\tau = \frac{1}{c}\sqrt{g_{\mu\nu}(x)\, dx^\mu dx^\nu}} \tag{2.1.2}$$

is interpreted as the time that records a comoving clock between x^μ and $x^\mu + dx^\mu$. Since, in general, the components of the metric depends on the coordinates, we see that in a curved spacetime the proper times recorded by clocks depend on velocities and positions in the spacetime.

On the other hand, based on the metric, it is possible to define the Christoffel connection defined as:

$$\Gamma^\alpha_{\beta\gamma} := \frac{1}{2} g^{\alpha\mu}\left[\partial_\gamma g_{\mu\beta} + \partial_\beta g_{\mu\gamma} - \partial_\mu g_{\beta\gamma}\right]. \tag{2.1.3}$$

Using the metric and the Christoffel connection we can define a geodesic, a generalization of the notion of a "straight line" to curved spaces. A geodesic satisfies the equation:

$$\boxed{\frac{d^2x^i}{d\lambda^2} + \Gamma^i_{jk}\frac{dx^j}{d\lambda}\frac{dx^k}{d\lambda} = f(\lambda)\frac{dx^i}{d\lambda},} \tag{2.1.4}$$

where λ is an arbitrary parameter. It is possible to choose a λ such that $f(\lambda) = 0$.

Additionally, the Riemann Curvature tensor is defined as

$$R^\rho_{\mu\nu\lambda} := \partial_\nu \Gamma^\rho_{\mu\lambda} - \partial_\lambda \Gamma^\rho_{\mu\nu} + \Gamma^\rho_{\sigma\nu}\Gamma^\sigma_{\mu\lambda} - \Gamma^\rho_{\sigma\lambda}\Gamma^\sigma_{\mu\nu}. \tag{2.1.5}$$

[1] 1pc $\approx$ 3.26ly $\approx 3.1 \times 10^{16}$m.

With those definitions Einstein formulated the fundamental equations of General Relativity as

$$G_{\mu\nu} := R_{\mu\nu} - \frac{1}{2}g_{\mu\nu}R - g_{\mu\nu}\Lambda = \frac{8\pi G}{c^4}T_{\mu\nu}, \tag{2.1.6}$$

where $R := R_{\mu\nu}g^{\mu\nu}$ is the Ricci scalar, Λ is the cosmological constant, $T_{\mu\nu}$ is the energy-momentum tensor of the system, c is the speed of light in vacuum and G is the Newtonian gravitational constant. From the definition of the Einstein tensor $G_{\mu\nu}$ and the Bianchi identities we see that the following equations are satisfied

$$\nabla_\mu T^{\mu\nu} = 0, \tag{2.1.7}$$

where ∇_μ is the covariant derivative defined as

$$\begin{aligned}\nabla_\mu T^{\alpha\beta\cdots}{}_{\gamma\delta\ldots} := \partial_\mu T^{\alpha\beta\cdots}{}_{\gamma\delta\ldots} + \Gamma^\alpha_{\epsilon\mu}T^{\epsilon\beta\cdots}{}_{\gamma\delta\ldots} + \Gamma^\beta_{\epsilon\mu}T^{\alpha\epsilon\cdots}{}_{\gamma\delta\ldots} + \cdots \\ - \Gamma^\epsilon_{\gamma\mu}T^{\alpha\beta\cdots}{}_{\epsilon\delta\ldots} - \Gamma^\epsilon_{\delta\mu}T^{\alpha\beta\cdots}{}_{\gamma\epsilon\ldots} - \cdots,\end{aligned} \tag{2.1.8}$$

where $T^{\alpha\beta\cdots}{}_{\gamma\delta\ldots}$ is a general tensor.

2.1.1 Dynamics of Friedmann-Lemaître-Robertson-Walker spacetime

Modern cosmology is the task of finding models from Einstein's field equations that are consistent with the large scale structures in the Universe. Modern observational cosmology has demonstrated that the Universe is highly symmetric in its large scale properties, but the evidence for this was not measured precisely at the time when Friedmann and Lemaître [1] began their pioneering investigations of the dynamics of a Universe with the simplest possible mass distribution, homogeneous and isotropic, using the Einstein's field equations. Subsequently these two assumptions (homogeneity and isotropy) would be called the Cosmological Principle. Furthermore, the current cosmology paradigm is based also in other assumption, in 1923 Hermann Weyl postulated that in cosmic spacetime there exists a set of privileged fundamental observers whose world lines are geodesic that do not intersect each other. This postulate implies that the proper time measured by each fundamental observer can be correlated with that of every other fundamental observer, allowing to associate a cosmic time with each event. At cosmological scales the Universe (seen by observers comoving with the cosmological fluid) is homogeneous and isotropic. The most general 4-dimensional metric that satisfy the cosmological principle is the Friedmann-Lemaître-Robertson-Walker (FLRW) metric. In spherical coordinates it is given by [1]

$$ds^2 = c^2dt^2 - a^2(t)\left[\frac{dr^2}{1-kr^2} + r^2d\theta^2 + r^2\sin^2\theta d\varphi^2\right], \tag{2.1.9}$$

where $a(t)$ is the cosmological scale factor and (t, r, θ, φ) are the coordinates of a comoving observer. The constant k can take the values $-1, 0$ or 1, corresponding to negative, null or positive curvature (of the spatial sections at constant t) respectively. More specifically, the 3D Ricci scalar curvature has value $R = 6k/a^2$.

To calculate the geodesic curves, first we must calculate the Christoffel connections. The non-null components for FLRW metric are:

$$\Gamma^0_{11} = \frac{1}{c}\frac{a\dot{a}}{1-kr^2}, \qquad \Gamma^0_{22} = \frac{1}{c}a\dot{a}r^2, \qquad \Gamma^0_{33} = \frac{1}{c}a\dot{a}r^2\sin^2\theta, \tag{2.1.10}$$

$$\Gamma^1_{01} = \frac{1}{c}\frac{\dot{a}}{a}, \qquad \Gamma^1_{11} = \frac{kr}{1-kr^2}, \qquad \Gamma^1_{22} = -r(1-kr^2), \tag{2.1.11}$$

$$\Gamma^1_{33} = -r(1-kr^2)\sin^2\theta, \qquad \Gamma^2_{02} = \frac{1}{c}\frac{\dot{a}}{a}, \qquad \Gamma^2_{12} = \frac{1}{r}, \tag{2.1.12}$$

$$\Gamma^2_{33} = -\sin\theta\cos\theta, \qquad \Gamma^3_{03} = \frac{1}{c}\frac{\dot{a}}{a}, \qquad \Gamma^3_{13} = \frac{1}{r}, \qquad \Gamma^3_{23} = \cot\theta. \tag{2.1.13}$$

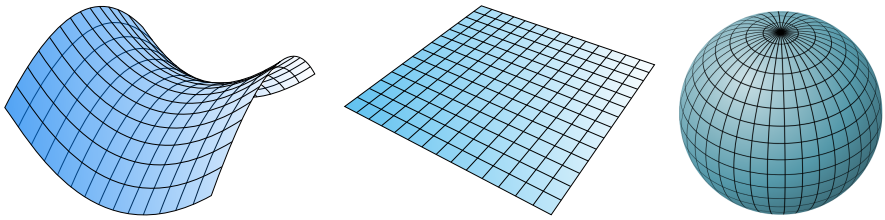

Figure 2.1: Examples of constant curvature 2D surfaces. At left there is a surface of negative curvature (hyperbolic paraboloid), in the central position there is a null curvature surface (plane) and at the right there is a positive curvature surface (sphere). Source: Own elaboration.

Now, since $\Gamma^{\mu}_{00} = 0$, the world line $x^{\mu}(\tau) = (c(\tau - \tau_0), r_0, \theta_0, \varphi_0)$ with τ_0, r_0, θ_0 and φ_0 constants, is a geodesic. Indeed,

$$\frac{dx^{\mu}}{d\tau} = (c, 0, 0, 0), \qquad \frac{d^2x^{\mu}}{d\tau^2} = 0, \tag{2.1.14}$$

satisfying the equation of the geodesic,

$$\frac{d^2x^{\mu}}{d\tau^2} + \Gamma^{\mu}_{\ \nu\lambda}\frac{dx^{\nu}}{d\tau}\frac{dx^{\lambda}}{d\tau} = 0 + \Gamma^{\mu}_{\ 00}c^2 = 0. \tag{2.1.15}$$

The cosmological fluid moves through geodesics of spacetime, corresponding to constant spacial coordinates. Thus, (2.1.9) implies that the temporal coordinate t coincides with the proper time. For this reason t is called *cosmological time*.

On the other hand, the energy-momentum tensor of the cosmological fluid needs to have these same properties of homogeneity and isotropy. Assuming that the cosmological fluid is a perfect fluid with isotropic pressure p and energy density ρ, the components of its energy-momentun tensor are

$$T^{00} = \rho(t), \qquad T^{0i} = 0, \qquad T^{ij} = -g^{ij}p(t), \qquad i, j = 1, 2, 3, \tag{2.1.16}$$

where the total preasure p and the total energy density ρ have only time dependence, due to homogeneity and the energy-momentum tensor is diagonal due to isotropy. From (2.1.7) we get

$$0 = \nabla_{\mu}T^{0\mu} = \partial_{\mu}T^{0\mu} + \Gamma^{0}_{\mu\nu}T^{\nu\mu} + \Gamma^{\mu}_{\mu\nu}T^{0\nu}, \tag{2.1.17}$$

$$= \partial_0 T^{00} + \Gamma^{0}_{ij}T^{ij} + \Gamma^{i}_{i0}T^{00}, \tag{2.1.18}$$

which corresponds to the balance equation

$$\boxed{\dot{\rho} + 3H(p + \rho) = 0,} \tag{2.1.19}$$

where $\dot{\rho} = d\rho/dt$ and $H = \dot{a}/a$ is the Hubble expansion rate that describes the evolution of the Universe. Using the Einstein equations we can obtain more information about the dynamics of the expansion of the Universe. From the 00 component of the Einstein field equations (2.1.6), considering $c = 1$, we get

$$\frac{3\ddot{a}}{a} = -4\pi G(\rho + 3p) + \Lambda, \tag{2.1.20}$$

and from the ij components we obtain

$$\frac{2k}{a^2} + \frac{2\dot{a}^2}{a^2} + \frac{\ddot{a}}{a} = 4\pi G(\rho - p). \tag{2.1.21}$$

Replacing (2.1.20) into (2.1.21) the second derivative of the scale factor can be removed, obtaining

$$\dot{a}^2 + k = \frac{8\pi G\rho a^2}{3} + \frac{\Lambda a^2}{3}. \tag{2.1.22}$$

This is the principal Friedmann equation, that describes the expansion of the Universe in terms of the total energy density ρ. It is important to note that without cosmological constant, the equation (2.1.20) implies that the Universe can only be decelerating (assuming $\rho > 0$ and $\rho + 3p > 0$, as it is for baryonic matter or radiation [2]).

On the other hand, the current data [3] indicates that the Universe has a null spatial curvature, i.e. $k = 0$, hence most of cosmological models do not consider the contribution of curvature in the dynamics of the cosmological expansion. Thus, Eq. (2.1.22) remains

$$\boxed{H^2 = \frac{8\pi G\bar{\rho}}{3},} \tag{2.1.23}$$

where $\bar{\rho}$ contains the cosmological constant term. Usually the change of variable $\bar{\rho} = (3H^2/8\pi G)\Omega$ is used, such that (2.1.23) is rewritten simply as

$$1 = \Omega. \tag{2.1.24}$$

The total energy density of the Universe is composed by different fluids such as baryonic matter, radiation, among others. Using (2.1.24) we can easily determine what percentage each energy density contributes to the total energy density in the Universe.

In order to describe the evolution of the acceleration of the Universe it is useful to define the "deceleration parameter"

$$q := -\frac{\ddot{a}a}{\dot{a}^2}, \tag{2.1.25}$$

which can be conveniently rewritten in terms of the Hubble expansion rate as

$$q = \frac{\dot{H}}{H^2} - 1. \tag{2.1.26}$$

The expansion of the Universe will be accelerated if $\ddot{a}$ is positive, and in this case the deceleration parameter will be negative. The minus sign and the name deceleration parameter are historical, when the parameter q was defined it was believed that the expansion of the Universe was decelerated.

2.2 Lambda Cold Dark Matter model

In 1917, Einstein included the cosmological constant in his field equations for G.R. because his equations do not allow a static Universe without the cosmological constant and he, as most scientist of his time, believed that the Universe must remain static. From Eq. (2.1.20) we see that in order to have a static Universe ($\ddot{a} = 0$) we need to include a positive cosmological constant (assuming $\rho + 3p \geq 0$). However, shortly after Einstein developed his static theory, observations by Edwin Hubble indicated that the Universe appears to be expanding, tearing down his model. Today data indicate that this expansion is accelerated and the cosmological constant is again considerate to obtain acceleration of the scale factor $\ddot{a} > 0$. The Lambda Cold Dark Matter model (ΛCDM) is a cosmological model in which the Universe contains a cosmological constant, denoted by Λ, which can be modeled as a perfect fluid with energy density $\rho_\Lambda = \Lambda/8\pi G$, and pressure $p_\Lambda = -\Lambda/8\pi G$. This is the simplest model that gives account of the accelerating expansion of the Universe. In this model it is assumed that the total energy density of the Universe is the result of the contributions of relativistic matter, dust and dark energy, where dark energy is modeled with the cosmological constant.

Current observations indicate that dust (Ω_m) corresponds to $4,9\%$ of baryonic matter (Ω_b) and an unknown type of matter, that do not emit radiation and remains undetected directly, it is called dark matter (Ω_DM) which contributes with a $26,8\%$ to the total energy density today. The remaining content of the Universe corresponds to dark energy modeled as cosmological

constant (Ω_Λ) with $68,3\%$. The contribution of radiation (Ω_r) is negligible today, but it was significant in the past [3], see Figure 2.2.

Although this model consistently explains the evolution of the Universe, it presents some problems that motivate us to explore new models generalizing some of its features.

- The Cosmological Constant Problem.

  The cosmological constant have an unknown nature, and have surged different explanations of its origin, but none has succeeded. In particular if we assume that dark energy comes from quantum vacuum energy density, it is obtained that it energy density is approximately $10^{74}\mathrm{GeV}^4$, but according to the current data, the approximate value of the energy density associated to the cosmological constant is $\rho_\Lambda \sim 10^{-47}\mathrm{GeV}^4$ [1]. This discrepancy has been called "the worst theoretical prediction in the history of physics!" [1]. On the other hand, another problem of cosmological constant is that this model does not explain the initial value of the energy densities associated to matter and cosmological constant. If acceleration of the Universe's expansion had began earlier, structures such as galaxies would never have had time to form and life, at least as we know it, would never have had a chance to exist. Modeling the dark energy as the cosmological constant it is not possible to satisfactorily answer this question.

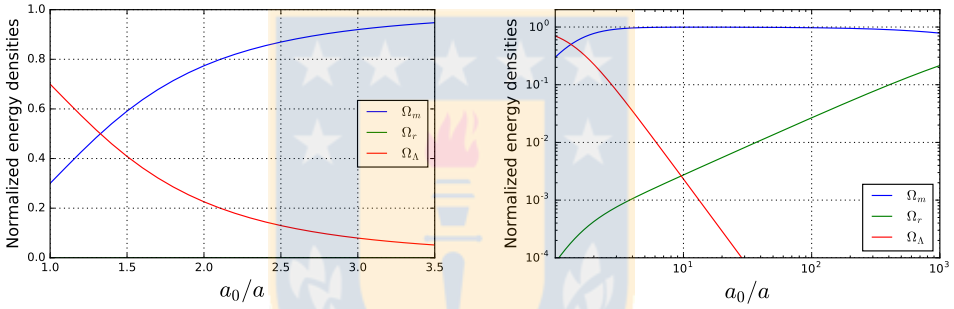

Figure 2.2: Graphics of the evolution of the normalized energy densities, matter (Ω_m), radiation (Ω_r) and cosmological constant (Ω_Λ). a_0 is the current value of the scale factor. At right, a loglog graphic it shown in order to note the contribution of the radiation component in the past. The value of the parameters today were taken from the Plank Collaboration [3]. Source: Own elaboration.

- The Coincidence Problem.

  Cosmological data indicate that we live in a period in the evolution of the Universe, when Ω_m and Ω_Λ are of the same order of magnitude. This raises a question: Why the energy density of cold dark matter and the constant energy density associated to Λ are of the same order today?. Thus, despite evolution of a over many orders of magnitude, we appear to live in an era during which the two energy densities values are roughly the same. In other words, at the beginning the dark energy density was negligible in comparison to dark matter and radiation energy densities, later in the Universe's evolution matter and radiation energy densities become negligible, there is only a brief epoch of the Universe's evolution during which it would occurs the transition from domination of dark matter to dark energy and it seems remarkable that we live during the transitional period between these two eras [1].

Besides the aforementioned theoretical problems, by contrasting ΛCDM model with the available data it is found some observational tensions recently reported, present when we use independently high redshift and low redshift data to constrain parameters [4].

2.3 Alternative models

To alleviate the cosmological constant problem and the coincidence problem different cosmological models have been proposed, within and outside the framework of General Relativity. Here we introduce some models within the framework of General Relativity. Since, these models do not consider dark energy as a constant necessarily, it is commonly used the subscript x, to denote dark energy components instead of the subscript Λ.

2.3.1 Omega Cold Dark Matter model

The ωCDM model is slightly more general than the ΛCDM model. In this model the dark energy is modeled as a barotropic perfect fluid with a constant parameter of state ω, whose value is determined using observational data.

In the description of the evolution of a cosmological scenario, we have two independent equations (2.1.20) and (2.1.22) and three unknown variables (a, ρ and p). Therefore, to solve these equations it is necessary to introduce an ansatz. The simplest and non-trivial assumption is to consider a barotropic equation of state with a constant parameter of state ω, i.e.

$$p = \omega\rho, \tag{2.3.1}$$

and solving (2.1.19) for ρ in terms of a, we get

$$\rho = \rho_0 \left(\frac{a}{a_0}\right)^{-3(1+\omega)}, \tag{2.3.2}$$

where a_0 is the current value of the scale factor. In the case that the cosmological fluid is mostly composed by dust ($p \ll \rho$), then $\omega \ll 1$ and therefore

$$\rho_{\rm m} = \rho_{\rm m0} \left(\frac{a}{a_0}\right)^{-3}. \tag{2.3.3}$$

On the other hand, if relativistic matter is predominant ($p = \rho/3$, i.e. $\omega = 1/3$), we have

$$\rho_{\rm r} = \rho_{\rm r0} \left(\frac{a}{a_0}\right)^{-4}. \tag{2.3.4}$$

Thus, for ωCDM model the total energy density is written as

$$\rho = \rho_{\rm r} + \rho_{\rm m} + \rho_{\rm x} \tag{2.3.5}$$

$$= \rho_{\rm r0} a^{-4} + \rho_{\rm m0} a^{-3} + \rho_{\rm x0} a^{-3(1+\omega)}, \tag{2.3.6}$$

where we have considered $a_0 = 1$ and $\rho_{\rm x0}$ corresponds to the current value of the dark energy density, we note that in the case $\omega = -1$ the ΛCDM model is recovered and $\rho_{\rm x0} \to \rho_\Lambda$.

It is worth to mention that from Eq. (2.1.20), when $\Lambda = 0$ and assuming a barotropic fluid as matter content, we can obtain an accelerated expansion when the effective parameter of state satisfies $\omega < -1/3$.

2.3.2 Dark Energy Parametrizations

Another possible scenario for dark energy is to consider a time-dependent equation of state, in other words, $p = \omega(t)\rho$. Future measurements could allow us study the behavior of $\omega(t)$ and for this reason, there are different parametrization of ω. In this section we present some aspects of these models.

Let us consider that the total cosmological fluid of the Universe is composed by radiation, dark matter and dark energy evolving independently. Then Eq. (2.1.19) can be separated in three equations, one for each fluid. In particular, for dark energy we have

$$\dot{\rho_{\rm x}} + 3H(1+\omega)\rho_{\rm x} = 0, \tag{2.3.7}$$

then, the Hubble expansion rate is given by

$$H^2 = H_0^2[\Omega_{\rm r0}a^{-4} + \Omega_{\rm m0}a^{-3} + \Omega_{\rm x0}f(a)], \tag{2.3.8}$$

where the subscript 0 means current values and

$$f(a) = \frac{\rho_{\rm x}(a)}{\rho_{\rm x0}} = \exp\left[3\int_{\frac{1-a}{a}}^{1}\frac{1+\omega(a')}{a'}da'\right]. \tag{2.3.9}$$

In Table 2.1 we show some parameterizations for the state parameter [5]:

Parametrization	$\omega(z)$	$f(z)$
Chevalier-Polarski-Linder (CPL)	$\omega_0 + \omega_1\frac{z}{1+z}$	$\exp\left(\frac{-3\omega_1 z}{1+z}\right)(1+z)^{3(1+\omega_0+\omega_1)}$
Jassal-Bagla-Padmanabhan	$\omega_0 + \omega_1\frac{z}{(1+z)^2}$	$(1+z)^{3(1+\omega_0)}\exp\left(\frac{3\omega_1 z^2}{2(1+z)^2}\right)$
Barbosa-Alcaniz	$\omega_0 + \omega_1\frac{z(1+z)}{(1+z)^2}$	$(1+z)^{3(1+\omega_0)}(1+z^2)^{3\omega_1/2}$
Feng-Shen-Li-Li	$\omega_0 + \omega_1\frac{z}{1+z^2}$	$(1+z)^{3(1+\omega_0)}\exp\left[\frac{3\omega_1}{2}\arctan(z)\right]$ $\times(1+z^2)^{3\omega_1/4}(1+z)^{-3\omega_1/2}$

Table 2.1: Parameterizations, where ω_0 and ω_1 are constants and $z+1 = a_0/a$. Source: Own elaboration.

Due to the fact that there is a large number of dark energy models, it is complicated to describe in detail each one of them. The parameterizations give us a simple idea of what the behavior of dark energy is and this allows us to extract the maximal information of the present value of the state parameter ω_0 and, where possible, its eventual time evolution.

2.3.3 Quintessence model

In this scenario dark energy is modeled by a scalar field. The first example of this scenario was proposed by Ratra and Peebles in 1988 [6]. Quintessence differs from the cosmological constant explanation because quintessence dark energy is dynamic, unlike the cosmological constant, which always remains constant. It is suggested that quintessence can behave as dark matter or dark energy depending on the ratio of it is kinetic and potential energy. Quintessence is a scalar field with an equation of state where $\omega_{\rm x}$, the ratio of pressure $p_{\rm x}$ and energy density $\rho_{\rm x}$, is given in terms of the potential energy $V(\varphi)$ and a kinetic term $\dot{\varphi}^2$:

$$\omega_{\rm x} = \frac{p_{\rm x}}{\rho_{\rm x}} = \frac{\frac{1}{2}\dot{\varphi}^2 - V(\varphi)}{\frac{1}{2}\dot{\varphi}^2 + V(\varphi)}. \tag{2.3.10}$$

The evolution of $\omega_{\rm x}$ can be known analytically in terms of a few model parameters. Using the analytical expression of $\omega_{\rm x}$, we can constrain quintessence models from the observational data. Furthermore, we note that the range of equation of state $\omega_{\rm x}$ is in the region $-1 \leq \omega_{\rm x} \leq 1$. When $\dot{\varphi}^2 \ll V(\varphi)$ we have $\omega_{\rm x} = -1$ giving a $\rho =$ const. and for $V(\varphi) \ll \dot{\varphi}^2$ we have $\omega_{\rm x} = -1$, in this case $\rho \propto a^{-6}$. Nevertheless, for an accelerated expansion of the Universe the parameter of state $\omega_{\rm x}$ must satisfy $-1 \leq \omega_{\rm x} \leq -1/3$.

2.4 Cosmological Interaction

Given that the nature of dark energy and dark matter is unknown and they dominate the energy content of the Universe today, it is reasonable to consider more general scenarios where dark matter and dark energy are phenomenologically coupled. Models based on the interaction between dark matter and dark energy have been studied to describe the accelerated expansion. One of the first interacting models was proposed in Ref. [7] mainly motivated to alleviate the coincidence problem in an interacting-quintessence scenario, focusing in an asymptotic attractor

behavior for the ratio of the energy densities for the dark components. Since then, many interacting models with numerical and analytical solutions have emerged [8], [9], [10] and [11], also interactions with change of sign have been studied in Refs. [12], [13], [14], [15] and [16]. A recent detailed review can be found in Ref. [17]. In particular Refs. [18] present analytical solutions for a wide class of more elaborated interactions where the dark components are barotropic fluids with constant state parameters. Also, the question of how to discriminate among dark energy models (degeneracy problem [19]) has arise in the context of interacting scenarios. In particular, there has been a debate on whether interacting models can be distinguished from modified dark energy equations of state, Chaplygin gas or modified gravity [20], which remains an open issue.

By separating Eq. (2.1.19) for dark matter and dark energy we get

$$\dot{\rho}_{\rm m} + 3H(\rho_{\rm m} + p_{\rm m}) = -Q, \tag{2.4.1}$$

$$\dot{\rho}_{\rm x} + 3H(\rho_{\rm x} + p_{\rm x}) = Q, \tag{2.4.2}$$

where the subscripts x and m denote the dark energy and the dark matter respectively. The function Q represents the interaction between these fluids. In the absence of a microscopic model for the interaction of dark matter and dark energy (i.e., an explicit form of Q), most proposed schemes are phenomenological. For $Q < 0$ the energy transfer is from dark energy to dark matter and for $Q > 0$ the energy transfer is from dark matter to dark energy today. It is common to choose Q as a function of ρ or combinations of $\rho_{\rm x}$ and $\rho_{\rm m}$ and its derivatives.

In order to find analytical solutions the set of Eqs. (2.4.1) and (2.4.2), we use the variable change $\eta := \ln a^3$ and $\Gamma := Q/3H$, obtaining

$$\rho'_{\rm m} + \gamma_{\rm m}\rho_{\rm m} = -\Gamma, \tag{2.4.3}$$

$$\rho'_{\rm x} + \gamma_{\rm x}\rho_{\rm x} = \Gamma, \tag{2.4.4}$$

with $\gamma_{\rm m} := 1 + \omega_{\rm m}$, $\gamma_{\rm x} := 1 + \omega_{\rm x}$ and $(\ \ )' = d(\ \ )/d\eta$.

From (2.4.3) and (2.4.4), and using that $\rho = \rho_{\rm x} + \rho_{\rm m}$ we can write $\rho_{\rm x}$ and $\rho_{\rm m}$ as a function of ρ and ρ' [21],

$$\rho_{\rm x} = \frac{\gamma_{\rm m}\rho + \rho'}{\Delta}, \qquad \rho_{\rm m} = -\frac{\gamma_{\rm x}\rho + \rho'}{\Delta}, \tag{2.4.5}$$

with $\Delta := \gamma_{\rm m} - \gamma_{\rm x}$. Using these equations we can obtain the "source equation" defined in [21],

$$\rho'' + (\gamma_{\rm x} + \gamma_{\rm m})\rho' + \gamma_{\rm x}\gamma_{\rm m}\rho = \Delta\Gamma. \tag{2.4.6}$$

It is important to emphasize that due to (2.4.5) and (2.4.6) every Γ proportional to $\rho_{\rm x}$ and/or $\rho_{\rm m}$ and/or its derivatives is in fact a differential equation for ρ.

It is interesting to note that by rewriting Eq. (2.4.6) as

$$\rho\left[\rho'' + b_1\rho' + b_3\rho\right] + b_2\rho'^2 = 0, \tag{2.4.7}$$

we include the eight types of interaction shown in Table 2.2 in a single differential equation, where the constants b_1, b_2, b_3 are different combinations of the relevant parameters depending on the particular interaction, see Table 2.2. The general solution of Eq. (2.4.7) takes the form

$$\rho(a) = \left[C_1 a^{\frac{3}{2}\lambda_1} + C_2 a^{\frac{3}{2}\lambda_2}\right]^{\frac{1}{1+b_2}}, \tag{2.4.8}$$

by using $\Omega_{\rm m0} + \Omega_{\rm x0} = 1$ and $\rho_0 = \rho_{\rm x0} + \rho_{\rm m0}$ we get that:

$$C_1 = -(3H_0^2)^{1+b_2}\left[\frac{\lambda_2 + \gamma_0(1+b_2)}{\lambda_1 - \lambda_2}\right], \tag{2.4.9}$$

$$C_2 = (3H_0^2)^{1+b_2}\left[\frac{\lambda_1 + \gamma_0(1+b_2)}{\lambda_1 - \lambda_2}\right], \tag{2.4.10}$$

and

$$\lambda_1 = -b_1 - \sqrt{b_1^2 - 4b_3(1+b_2)}, \tag{2.4.11}$$

$$\lambda_2 = -b_1 + \sqrt{b_1^2 - 4b_3(1+b_2)}, \tag{2.4.12}$$

$$\gamma_0 = \gamma_{\rm m} - \Omega_{\rm x0}\Delta. \tag{2.4.13}$$

Interaction	b_1	b_2	b_3
$\Gamma_1 = \alpha\rho_{\rm m} + \beta\rho_{\rm x}$	$\gamma_{\rm m} + \gamma_{\rm x} + \alpha - \beta$	0	$\gamma_{\rm m}\gamma_{\rm x} + \alpha\gamma_{\rm x} - \beta\gamma_{\rm m}$
$\Gamma_2 = \alpha\rho'_{\rm m} + \beta\rho'_{\rm x}$	$\frac{\gamma_{\rm m} + \gamma_{\rm x} + \alpha\gamma_{\rm x} - \beta\gamma_{\rm m}}{1+\alpha-\beta}$	0	$\frac{\gamma_{\rm m}\gamma_{\rm x}}{1+\alpha-\beta}$
$\Gamma_3 = \alpha\rho_{\rm m}\rho_{\rm x}/(\rho_{\rm m} + \rho_{\rm x})$	$\gamma_{\rm m} + \gamma_{\rm x} + \alpha\frac{\gamma_{\rm m} + \gamma_{\rm x}}{\Delta}$	$\frac{\alpha}{\Delta}$	$\gamma_{\rm m}\gamma_{\rm x} + \alpha\frac{\gamma_{\rm m}\gamma_{\rm x}}{\Delta}$
$\Gamma_4 = \alpha\rho_{\rm m}^2/(\rho_{\rm m} + \rho_{\rm x})$	$\gamma_{\rm m} + \gamma_{\rm x} - \frac{2\alpha\gamma_{\rm x}}{\Delta}$	$-\frac{\alpha}{\Delta}$	$\gamma_{\rm m}\gamma_{\rm x} - \frac{\alpha\gamma_{\rm x}^2}{\Delta}$
$\Gamma_5 = \alpha\rho_{\rm x}^2/(\rho_{\rm m} + \rho_{\rm x})$	$\gamma_{\rm m} + \gamma_{\rm x} - \frac{2\alpha\gamma_{\rm m}}{\Delta}$	$-\frac{\alpha}{\Delta}$	$\gamma_{\rm m}\gamma_{\rm x} - \frac{\alpha\gamma_{\rm m}^2}{\Delta}$
$\Gamma_6 = \alpha\rho$	$\gamma_{\rm m} + \gamma_{\rm x}$	0	$\gamma_{\rm m}\gamma_{\rm x} - \alpha\Delta$
$\Gamma_7 = \alpha\rho'$	$\gamma_{\rm m} + \gamma_{\rm x} - \alpha\Delta$	0	$\gamma_{\rm m}\gamma_{\rm x}$
$\Gamma_8 = \alpha q\rho = -\alpha(\rho + \frac{3}{2}\rho')$	$\gamma_{\rm m} + \gamma_{\rm x} + \frac{3}{2}\alpha\Delta$	0	$\gamma_{\rm m}\gamma_{\rm x} + \alpha\Delta$

Table 2.2: Expressions for the constants b_1, b_2 and b_3 for the considered interaction. Source: Own elaboration.

On the other hand, in order to analyze the evolution of the energy densities and the coincidence problem we use the coincidence parameter r defined as

$$r := \frac{\rho_{\rm m}}{\rho_{\rm x}}. \tag{2.4.14}$$

In the case of ΛCDM model, since ρ_Λ is constant and $\rho_{\rm m}$ decreases proportional to a^{-3}, then r decrease (asymptotically to 0) when a increase. This means that today is a very particular epoch in the evolution of the Universe, whereas if for example r tends to a constant different of 0 it means that today is not a very particular epoch, since dark matter and dark energy at late Universe evolve at the same rate. In [21], the author analyzes some linear and nonlinear interactions proportional to the energy densities, concluding that interacting functions that include a linear term proportional to $\rho_{\rm x}$, alleviate the coincidence problem when the parameter $\gamma_{\rm x} > 0$.

2.5 Observational Cosmology

One of the first observational data used to study the behavior of the Universe dates from 1929. Edwin Hubble used Cepheids, a type of variable star that pulsates radially, varying in both temperature and diameter to produce brightness changes with a well defined period and amplitude, as a mean to determine distances, to study the properties of the Universe. Hubble was the first to account for the cosmological expansion [22] (see Figure 2.3), but their observations were not precise enough to determine whether it is an accelerating or a decelerating expansion.

Due to this discovery, new questions about the Universe arise. For example, if the Universe is expanding, does that means that it had a beginning? Moreover, will the Universe have an ending as well? To answer this and other questions it is necessary to have more information about the Universe. In 1965 Arno Penzias and Robert Woodrow Wilson in the Bell Laboratories

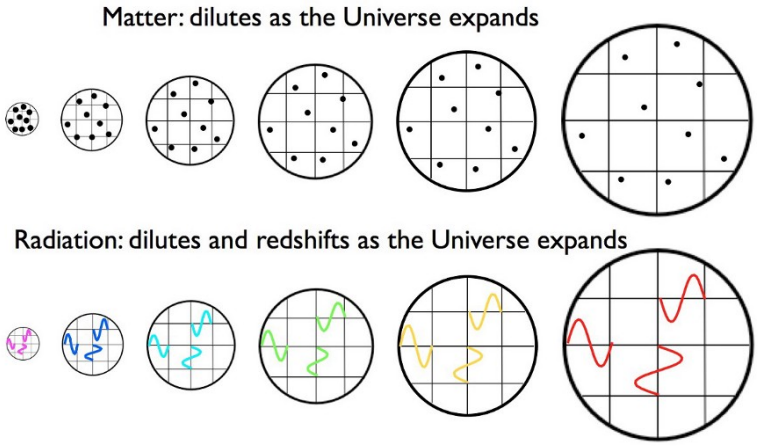

Figure 2.3: Scheme of the Universe's expansion. Matter and radiation dilute in an expanding Universe; note the radiation's redshift to lower and lower energies over time. Source: Extracted from `https://goo.gl/VLZAVo`.

detected for the first time the Cosmic Microwave Background (CMB) [23]. This radiation was predicted by George Gamow, Ralph Alpher and Robert Hermann in 1948. The CMB is the thermal radiation left over from the time of recombination in Big Bang theory.

The CMB radiation has a blackbody spectrum, i.e., it is a type of electromagnetic radiation emitted by a body in thermodynamic equilibrium with its environment. The radiation has a specific spectrum and intensity that depends only on the temperature of the body.

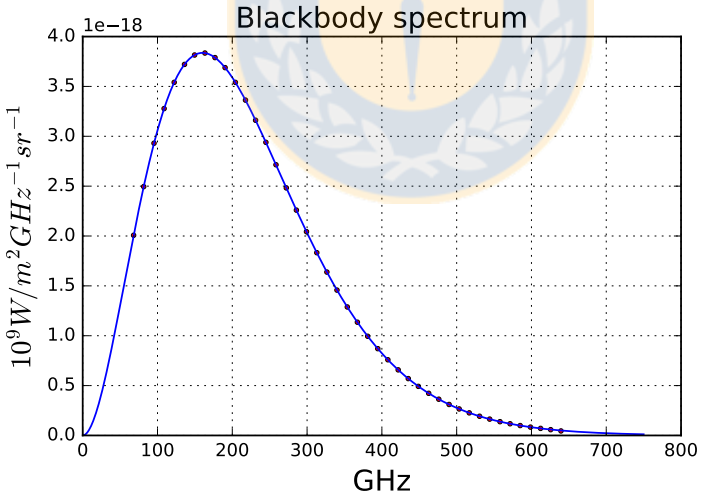

Figure 2.4: CMB spectrum. The points are observational data from CMB taken by the COBE satellite and the curve corresponds to an ideal blackbody spectrum at temperature of $2.725K$. Source: Own elaboration.

With the CMB detection, the Big Bang theory became more accepted and in a few years it became part of the standard cosmological model. In 1978, Arno Penzias and Robert Wilson won the Physics Nobel Prize for the CMB detection. In 1989, the COBE satellite was launched to investigate the CMB properties and after that, other satellites were launched with this same purpose: the WMAP satellite in 2001 and the Planck satellite in 2009, increasing the accuracy in the measurement of the temperature's anisotropies of the CMB.

In 1998, contrary to what was expected (that the expansion of the Universe was slowing down) the High-z Supernova Search Team led by Adam G. Riess reported the first evidence of the current accelerated expansion of the Universe through monitoring of type Ia Supernovae [24]. The results of High-z Supernova Search Team were also found nearly simultaneously by the Supernova Cosmology Project, led by Saul Perlmutter [25]. The corroborating evidence between the two competing studies led to the acceptance of the accelerating Universe, and initiated new research to understand the Universe's expansion and dark energy nature.

A type Ia Supernova is a type of supernova that occurs in binary systems (two stars orbiting one another) in which one of the stars is a white dwarf. The other star can be anything from a giant star to an even smaller white dwarf. This type Ia category of supernovae produces a characteristic luminosity peak because of the uniform mass of white dwarfs that explode via the accretion mechanism. The light curve of type Ia supernovae allows to these explosions to be used as standard candles to measure the distance to their host galaxies because the visual magnitude of the supernovae depends primarily on the distance [1].

The discovery of the accelerating expansion of the Universe awarded Riess the 2011 Nobel Prize in Physics along with Schmidt and Perlmutter, "For the discovery of the accelerating expansion of the Universe through observations of distant Supernovae". It is worth to mention the contribution of the Calán/Tololo Survey in Chile, a team led by Mario Hamuy, with Mark Philips, Nick Suntzeff (of the Cerro Tololo Inter-American Observatory in Chile), Robert Schommer, Jose Maza who were conducting the first large-scale program, measuring the light curves of type Ia supernovae. These data were essential to demonstrate that type Ia SNe were useful as standard candles. Progress was made using a relation between peak brightness and fading time, shown by Mark Phillips, to recalibrate the SNe to a standard profile. Currently there are different supernovae survey dedicated to detecting and monitoring high-redshift supernovae to investigate dark energy and the accelerated expansion of the Universe [26].

2.5.1 Distance indicators

At a cosmological level, the measurements of distance allow us to learn about the Universe both in its size and age, through the cosmological expansion [1]. From Special Relativity we know that distance is not an absolute magnitude; this depends on the observer. In cosmology there are many differents definitions of distance, each one useful depending on what is to be measured.

Cosmological Redshift

Consider two light rays emanated from a point P at cosmological time t_1 and $t_1 + \delta t_1$, and received by the observer O at t_0 and $t_0 + \delta t_0$ respectively as is shown in Figure 2.5. Using the FLRW metric (2.1.9) we can describe the trajectory of the radial photons traveling in the spacetime, given that $ds^2 = 0$ and θ and φ are constants we obtain that

$$c\int_{t_1+\delta t_1}^{t_0+\delta t_0} \frac{dt}{a(t)} = -\int_{r_1}^{r_0} \frac{dr}{\sqrt{1-kr^2}}. \tag{2.5.1}$$

Assuming that the radial comoving coordinate r of the light source and the receptor remains constant, the right side of equation (2.5.1) remains the same even considering other emission and reception time on the left side. In particular, if we consider the interval from t_1 to t_0 we get

$$\int_{t_1}^{t_0} \frac{dt}{a(t)} = \int_{t_1+\delta t_1}^{t_0+\delta t_0} \frac{dt}{a(t)}, \tag{2.5.2}$$

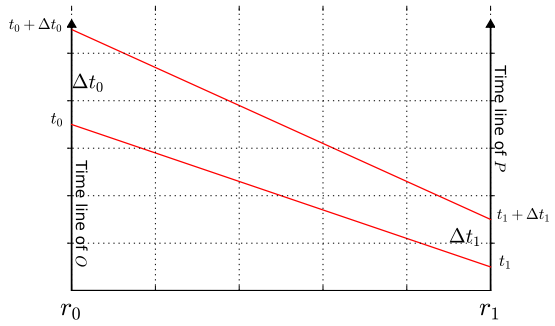

Figure 2.5: Scheme where P point sends light rays to the point O. Source: Own elaboration.

passing the integral on the left side and separating them we get that

$$0 = -\int_{t_1}^{t_0} \frac{dt}{a(t)} + \int_{t_1+\delta t_1}^{t_0} \frac{dt}{a(t)} + \int_{t_0}^{t_0+\delta t_0} \frac{dt}{a(t)}, \tag{2.5.3}$$

$$= \int_{t_0}^{t_1} \frac{dt}{a(t)} + \int_{t_1+\delta t_1}^{t_0} \frac{dt}{a(t)} + \int_{t_0}^{t_0+\delta t_0} \frac{dt}{a(t)}, \tag{2.5.4}$$

$$= -\int_{t_1}^{t_1+\delta t_1} \frac{dt}{a(t)} + \int_{t_0}^{t_0+\delta t_0} \frac{dt}{a(t)}. \tag{2.5.5}$$

Assuming that $a(t)$ changes negligibly between δt_1 and δt_0 ($\delta t_0 \ll a/\dot{a}$ and $\delta t_1 \ll a/\dot{a}$), we can find a relation at first order in δt_1 and δt_0 from (2.5.5):

$$\frac{\delta t_0}{a(t_0)} = \frac{\delta t_1}{a(t_1)}. \tag{2.5.6}$$

Further, we can relate δt_1 and δt_0 with frequencies, considering them as periods of emission, thus $\delta t_1 = 1/\nu_1$ and $\delta t_0 = 1/\nu_0$. By using the definition of redshift $z = \frac{\nu_{\text{emitted}}}{\nu_{\text{received}}} - 1$ can find an expression for the cosmological redshift z in term of $a(t)$ from (2.5.6):

$$\boxed{z = \frac{a(t_0)}{a(t)} - 1,} \tag{2.5.7}$$

where we have generalized t_1 to an arbitrary cosmic time t. From this last equation we see that $z = 0$ represents today, $z \to \infty$ represents the Big Bang epoch and $-1 < z < 0$ means a future epoch.

Comoving distance

Using the FLRW metric (2.1.9) in photons traveling in the spacetime in a radial trajectory we get

$$\frac{cdt}{a(t)} = -\frac{dr}{\sqrt{1-kr^2}}, \tag{2.5.8}$$

and through (2.5.7) we obtain

$$\frac{cdz}{H(z)} = \frac{dr}{\sqrt{1-kr^2}}, \tag{2.5.9}$$

considering $a(t_0) = a_0 = 1$. The comoving distance d_c is defined as

$$d_c(z) := \int_0^r \frac{dr'}{\sqrt{1-kr'^2}} = d_H \int_0^z \frac{dz'}{E(z')}, \tag{2.5.10}$$

where $d_H := c/H_0$, $E(z) := H(z)/H_0$ so that

$$E^2(z) := \Omega_{\rm x}(z) + \Omega_{\rm k0}(1+z)^2 + (\Omega_{\rm DM0} + \Omega_{\rm b0})(1+z)^3 + \Omega_{\rm r0}(1+z)^4, \tag{2.5.11}$$

where $\Omega_{\rm DM0}$ corresponds to the normalized dark matter energy density and $\Omega_{\rm b0}$ corresponds to the baryons energy density. The subscript 0 means current values. The subindex k is related to the curvature of space, and $\Omega_{\rm k0} = -k/H_0^2$.

Radial Coordinate

We can obtain the radial coordinate of an object at redshift z from equation (2.5.9), this quantity is related to the comoving distance $d_c(z)$ by

$$r(z) := \begin{cases} \dfrac{d_H}{\sqrt{\Omega_{\rm k}}} \sinh\left(\dfrac{\sqrt{\Omega_{\rm k}} d_c(z)}{d_H}\right), & \text{for} \quad \Omega_{\rm k} > 0 \\ d_c(z) \qquad\qquad , & \text{for} \quad \Omega_{\rm k} = 0 \\ \dfrac{d_H}{\sqrt{\Omega_{\rm k}}} \sin\left(\dfrac{\sqrt{\Omega_{\rm k}} d_c(z)}{d_H}\right), & \text{for} \quad \Omega_{\rm k} < 0 \end{cases} . \tag{2.5.12}$$

Angular diameter distance

A common way to determine distances in Astronomy is to measure the angle $\delta\theta$ subtended by an object of known physical size X at redshift z. The angular diameter distance D_A is defined as the ratio of an object's physical size to its angular size (in radians), i.e. $D_A(z) := X/\delta\theta$ [27]. This is commonly used in the context of Baryon Acoustic Oscillations. To compute the angular diameter distance in an expanding Universe, we first note that the comoving size of the object is X/a, where a is the cosmological scale factor. On the other hand, the comoving distance to the object is given by equation (2.5.12), so the angle subtended is $\delta\theta = (X/a)/d_c$. The angular diameter distance is related to the radial coordinate (for $k = 0$) as

$$D_A := \frac{r(z)}{1+z}, \tag{2.5.13}$$

where we have used (2.5.7).

2.5.2 Apparent Magnitude

This is the most useful method to determine distances in Cosmology. It is based on the measurement of the apparent luminosity of objects with known absolute luminosity. The absolute luminosity L is the energy emitted per unit of time. Then, assuming that the energy is emitted isotropically, the total power per unit area l passing through a sphere of radius d centred at the object (in an Euclidean space) is

$$l = \frac{L}{4\pi d^2}. \tag{2.5.14}$$

In practice, it is important to consider the effect of the atmosphere in the luminosity, because it absorbs a portion of the apparent luminosity. The bolometric magnitude is defined as the magnitude of an object adjusted to the value it would have in absence of the atmosphere. The absolute and apparent magnitude M and m are given by [1]

$$l = 10^{-2m/5} \times 2.52 \times 10^{-5} \left[\frac{\rm erg}{\rm cm^2 s}\right], \tag{2.5.15}$$

and

$$L = 10^{-2M/5} \times 3.02 \times 10^{35} \left[\frac{\rm erg}{\rm s}\right]. \tag{2.5.16}$$

Using these equations we can rewrite (2.5.14) as

$$d = 10^{1+(m-M)/5} \text{ [pc]}. \tag{2.5.17}$$

It is important to mention that these equations do not include effects associated to the expansion of the Universe, for this we must consider the metric FLRW in our calculations of distances.

Luminosity distance

Let us imagine a star with coordinates $x_1^\mu = (ct_1, r_1, 0, 0)$, and the Earth with coordinates $x_0^\mu = (ct_0, 0, 0, 0)$. Using (2.1.9), the metric induced on a sphere centred (for a fixed time) in x_1^μ and passing through x_0^μ is

$$dl^2 = a_0^2 r_1^2 (d\theta^2 + \sin^2\theta d\varphi^2), \qquad \text{with} \qquad a_0 = a(t_0), \tag{2.5.18}$$

whose area is

$$A = 4\pi a_0^2 r_1^2. \tag{2.5.19}$$

Furthermore, if the star emits J photons with frequency ν_1, in a time interval δt_1, the absolute luminosity is given by

$$L = \frac{Jh\nu_1}{\delta t_1} \quad \Rightarrow \quad J = \frac{L\delta t_1}{h\nu_1}, \tag{2.5.20}$$

with h the Planck constant. An observer at x_0^μ detects n photons (with $n < J$ and frequency ν_0) in an area S, in a time interval δt_0. In addition, since space is isotropic, any observer located on the spherical surface will receive the same number n of photons with frequency ν_0 during of the same time interval δt_0. Thus, assuming no loss of these photons, J photons will pass this surface in the time interval δt_0, i.e.

$$\int_A \frac{n}{S} dA = 4\pi a_0^2 r_1^2 \frac{n}{S} = J. \tag{2.5.21}$$

Then, we can rewrite the apparent luminosity as

$$l = \frac{nh\nu_0}{S\delta t_0} = \frac{Jh\nu_0}{4\pi a_0^2 r_1^2 \delta t_0}. \tag{2.5.22}$$

Replacing J from (2.5.20) into (2.5.22) we get

$$l = \frac{L}{4\pi a_0^2 r_1^2} \frac{\delta t_1}{\delta t_0} \frac{\nu_0}{\nu_1}. \tag{2.5.23}$$

Then using (2.5.6) and (2.5.7), we find the relation

$$l = \frac{L}{4\pi a_0^2 r_1^2 (1+z)^2}. \tag{2.5.24}$$

Based on this result, we can define the luminosity distance as

$$d_L := a_0 r_1 (1+z), \tag{2.5.25}$$

such that

$$l = \frac{L}{4\pi d_L^2}. \tag{2.5.26}$$

On the other hand, using (2.5.25) and (2.5.17) we can write the luminosity distance in terms of the relative and absolute magnitude as

$$\mu := m - M = 5\log_{10}\left(\frac{d_L}{\text{Mpc}}\right) + 25, \tag{2.5.27}$$

where μ is the so-called *distance modulus*.

The type Ia supernovae (SN Ia) can be observed when white dwarf stars, accreting mass from a companion star in a binary system approach the Chandrasekhar mass ($M_{\rm Ch} \approx 1.38$ solar masses), high temperature causes the ignition of explosive nuclear burning reactions [28]. SN Ia are formed in the same way irrespective of where they are in the Universe, which means that they have a common absolute magnitude M independent of the redshift z. Thus, they can be used as standard candles since we can measure the apparent magnitude m and the redshift z. Some recent compilations of supernovae are Union 2, Union 2.1 [29], Constitution [30] and JLA [26]. Since the first type Ia supernovae measurements to the present, the data sets of this supernovae have significantly grown. In 2008 the Constitution data set was compiled with 397 type Ia supernovae, in 2010 came Union 2 with 557 supernovae, one year later Union 2.1 arrived with 580 type Ia supernovae and JLA (Joint Light-curve Analyzis) arrived in 2014 with 740 type Ia supernovae.

2.5.3 Hubble function

The ΛCDM model assumes the dark energy density to be constant, but we can consider more general cases, for example, in which dark energy is modeled as a fluid with an equation of state, $p_{\rm x}(z) = (\gamma_{\rm x}(z) - 1)\rho_{\rm x}$, where the state function $\gamma_{\rm x}(z) - 1$ indicates the ratio between the pressure, $p_{\rm x}$, and the energy density, $\rho_{\rm x}$, of dark energy. Therefore, to determine the evolution of $\gamma_{\rm x}(z) - 1$ as a function of redshift we need to use precise measurements at redshifts when the dark energy started to dominate the expansion of the Universe [31].

The common approach for determining $\gamma_{\rm x}(z) - 1$ uses its effect on the luminosity distance of sources. To measure the luminosity distance, it is usual to use type Ia supernovae as standard candles. However, the sensitivity of the luminosity distance to the redshift history of $\gamma_{\rm x}(z) - 1$ is compromised by its integral nature, see equation (2.5.10). However, if we measure the age difference, Δt, between two passively-evolving galaxies that formed at the same time but separated by a small redshift interval Δz, one can infer the value of the derivative, (dz/dt), from the ratio $(\Delta z/\Delta t)$. The statistical significance of the measurement can be improved by selecting samples of passively-evolving galaxies at the two redshifts and by comparing the upper cut-off of their age distributions. All selected galaxies need to have similar metallicities and low star formation rates, so that the average age of their stars would far exceed the age difference between the two galaxy samples, Δt [31]. The quantity measured in this case is directly related to the Hubble parameter by

$$H(z) = -\frac{1}{1+z}\frac{dz}{dt}. \tag{2.5.28}$$

This differential age method is much more reliable than a method based on an absolute age determination for galaxies, given the integral nature of this last method. The more recent compilation of $H(z)$ data has 28 data points of H v/s z and it is found in Ref. [31].

2.5.4 Baryonic Acoustic Oscillations

Before the decoupling the Universe consisted of a hot plasma of photons, baryons, electrons and dark matter. The tight coupling between photons and electrons due to Thompson scattering leads to oscillations in the hot plasma. As the Universe expands and cools, electrons and nuclei combine into atoms making the Universe electrically neutral. Initial fluctuations in density and gravitational potential drive acoustic waves in the fluid (compressions and rarefactions). That relieved the pressure on the system, leaving behind a shell of baryonic matter at a fixed radius. This radius is often referred to as the sound horizon [32]. Many anisotropies created ripples in the density of space that attracted matter and eventually galaxies formed in a similar pattern. Therefore, one would expect to see a greater number of galaxies separated by the sound horizon. This effect can be seen in the spectrum of galaxy correlations today. The detection of imprints of these oscillations in the galaxy correlation function is difficult as the signal is suppressed by the fractional energy density of baryons which is about 4% of the total cosmic budget, but

the detection of these acoustic oscillations confirms several basic assumptions of cosmological structure formation theory and it also points the way to a new application of large-scale structure surveys for the study of dark energy.

The BAO scale is set by the radius of the sound horizon at the drag epoch z_d when photons and baryons decouple,

$$r_d = \int_{z_d}^{\infty} \frac{c_s(z)dz}{H(z)}, \tag{2.5.29}$$

where the sound speed in the photon-baryon fluid is [1]

$$c_s(z) = \frac{c}{\sqrt{3(1+\mathcal{R})}}, \tag{2.5.30}$$

where

$$\mathcal{R} := \frac{3\rho_{\rm b}}{4\rho_\gamma} = \frac{3\Omega_{\rm b}h^2}{9.88\times10^{-5}}\frac{1}{1+z}, \tag{2.5.31}$$

using that the normalized energy density of the CMB radiation is $\Omega_\gamma = 2.47\times10^{-5}h^{-2}$ [1].

To fit z_d we use the formula proposed by Eisenstein [32]

$$z_d = \frac{1291(\Omega_{\rm b}h^2)^{0.251}}{1+0.659(\Omega_{\rm m}h^2)^{0.828}}[1+b_1(\Omega_{\rm b}h^2)^{b_2}], \tag{2.5.32}$$

with

$$b_1 = 0.313(\Omega_{\rm m}h^2)^{-0.419}[1+0.607(\Omega_{\rm m}h^2)^{0.674}], \tag{2.5.33}$$

$$b_2 = 0.238(\Omega_{\rm m}h^2)^{0.223}. \tag{2.5.34}$$

Until now, we do not measure clustering directly in comoving space, but we instead measure galaxy redshifts, angles and infer distances from these.

In the radial direction, provided that the clustering signal is small compared with the cosmological distortions, the measurements are sensitive to the Hubble parameter through $1/H(z)$. In the angular direction the distortions depend on the angular diameter distance $D_A(z)$. Adjusting the cosmological model to ensure that angular and radial clustering match constrains $H(z)D_A(z)$, and was first proposed as a cosmological test (the AP test) by Alcock and Paczynski [33]. If we instead consider averaging clustering in 3D over all directions, then, to first order, matching the scale of clustering measurements to the comoving clustering expected is

$$D_{\rm v}(z) = \frac{1}{H_0}\left[(1+z)^2 D_A^2(z)\frac{cz}{E(z)}\right]^{\frac{1}{3}}, \tag{2.5.35}$$

although this projection applies to all of the clustering signal, BAO give the most robust and strongest source for the comparison between observed and expected clustering, providing a distinct feature on sufficiently large scales. Where $D_A(z)$ is the angular diameter. This quantity can be measured and compared to different cosmological models.

Other important function is the Acoustic Parameter $A(z)$ introduced by Eisenstein [32], defined by

$$A(z) := \frac{D_{\rm v}(z)\sqrt{\Omega_m H_0^2}}{cz}. \tag{2.5.36}$$

We note that $A(z)$ has no direct dependency on the Hubble constant H_0, since $D_{\rm v}$ is proportional to H_0^{-1}, this combination is well constrained by the data [34].

2.5.5 Cosmic Microwave Background

The Cosmic Microwave Background (CMB) is the radiation left over from the time of recombination. The CMB is a cosmic radiation that is fundamental to observational cosmology because it is a snapshot of the oldest radiation in our Universe, when the Universe was approx 380,000

years old. It shows tiny temperature fluctuations that correspond to regions of slightly different densities, representing the seeds of all observed structure.

The characteristic acoustic scale θ_A of the peaks on the angular power spectrum of the CMB anisotropies is defined as

$$\theta_A := \frac{\pi}{l_A} = \frac{r_s(z_{\rm dec})}{r(z_{\rm dec})}, \tag{2.5.37}$$

where $r_s(z_{\rm dec})$ is the comoving size of the sound horizon at decoupling, $r(z_{\rm dec})$ the comoving distance at decoupling and l_A the multipole associated with the angular scale θ_A [35]. The Figure 2.6 is the angular power spectrum of the CMB temperature, where we can see the peaks of the CMB anisotropies. Then, we can rewrite the equation (2.5.37) as

$$l_A = \frac{\pi d_L(z_{\rm dec})}{(1+z) r_s(z_{\rm dec})}. \tag{2.5.38}$$

Moreover, the redshift at decoupling is given by [36]

$$z_{\rm dec} = 1048[1 + 0.00124(\Omega_b h^2)^{-0.738}][1 + g_1(\Omega_b h^2)^{g_2}], \tag{2.5.39}$$

where

$$g_1 = \frac{0.0783(\Omega_b h^2)^{-0.238}}{1 + 39.5(\Omega_b h^2)^{0.763}}, \qquad g_2 = \frac{0.560}{1 + 21.1(\Omega_b h^2)^{1.81}}. \tag{2.5.40}$$

Another observable is the "shift parameter" R defined as [37], this parameter together with the sound horizon determine the location of the first peak at recombination

$$R = \frac{\sqrt{\Omega_m}}{c(1+z_{\rm dec})} D_L(z), \tag{2.5.41}$$

where $D_L(z) = H_0 d_L$. The data sets for anisotropies in the CMB radiation are publicly available in Ref. [34]. The data from CMB are given through the covariance matrix C as: $\chi^2_{\rm CMB} = X^{\rm T} C^{-1}_{\rm CMB} X$ [34] where

$$C^{-1}_{\rm CMB} = \begin{pmatrix} 3.182 & 18.253 & -1.429 \\ 18.253 & 11887.879 & -193.808 \\ -1.429 & -193.808 & 4.556 \end{pmatrix}. \tag{2.5.42}$$

and

$$X = \begin{pmatrix} l_A - 302.40 \\ R - 1.7246 \\ z_{dec} - 1090.88 \end{pmatrix}. \tag{2.5.43}$$

All these definitions are useful to test the cosmological models and determine how well they describe the Universe both in the present and in their past, allowing us to improve our understanding of it.

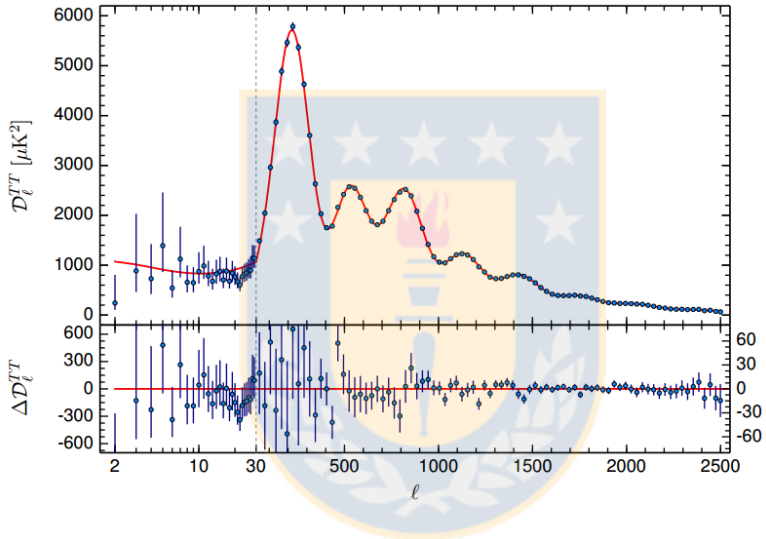

Figure 2.6: Planck 2015 temperature power spectrum. The blue points are the measured data and the red curve corresponds to the standard model of cosmology [3]. Source: Extracted from [3].

Chapter 3

Data Fitting and Model Comparison

Physics is based on the scientific method, which has as its cornerstone the observation of nature, but how can we connect what we perceive with our theories? The answer is not simple. Through measurements we can contrast the behavior of nature with our models of it. This process is a fundamental part of Science and specially in Physics allows us to better understand the physical phenomena and the laws of Nature. In the words of Richard Feynman: "The principle of Science, the definition, almost, is the following: *The test of all knowledge is experiment.* Experiment is the *sole judge* of scientific *truth*" [38].

Statistics investigates and develops specific methods for evaluating hypotheses in the light of empirical facts. A method is called statistical, and thus the subject of study in statistics, if it relates facts and hypotheses of a particular kind: the empirical facts must be codified and structured into data sets, and the hypotheses must be formulated in terms of probability distributions over possible data sets. The philosophy of statistics concerns the foundations and the proper interpretation of statistical methods, their input, and their results. Since statistics is relied upon in almost all empirical scientific research, serving to support and communicate scientific findings, the philosophy of statistics is of key importance to the philosophy of science.

Statistics is a mathematical and conceptual discipline that focuses on the relation between data and hypotheses. The data are recordings of observations or events in a scientific study, e.g., a set of measurements of individuals from a population. The data actually obtained are variously called the sample, the sample data, or simply the data, and all possible samples from a study are collected in what is called a sample space. The hypotheses, in turn, are general statements about the target system of the scientific study, e.g., expressing some general fact about all individuals in the population. A statistical hypothesis is a general statement that can be expressed by a probability distribution over sample space, i.e., it determines a probability for each of the possible samples.

Statistical methods provide the mathematical and conceptual means to evaluate statistical hypotheses in the light of a sample. To this aim they employ probability theory, and incidentally generalizations thereof. The evaluations may determine how believable a hypothesis is, whether we may rely on the hypothesis in our decisions, how strong the support is that the sample gives to the hypothesis.

3.1 Maximum Likelihood

In Statistics, Maximum Likelihood is a method of estimating the parameters of a statistical model given some data. The method of maximum likelihood corresponds to many well-known estimation methods in statistics. Maximum Likelihood would do this by taking the mean and variance as parameters and finding particular parametric values that make the observed results

the most probable given the model.

Suppose that we have a set of N data points corresponding to measurements of the independent variable x_i and the dependent variable y_i, with $i = 1, \ldots, N$ and we want to find the parameters $\mathbf{a} = [a_1, a_2, \ldots, a_I]$ of the model $y(x_i) \equiv y(x_i, \mathbf{a})$ that will fit to the data.
Then, for each event (x_i, y_i) we can transform the $y(x)$ function in a normalized probability density

$$P_i := P(x_i, \mathbf{a}). \tag{3.1.1}$$

Then, the **likelihood function** $\mathcal{L}(\mathbf{a})$ will be the product of the probability densities

$$\mathcal{L}(\mathbf{a}) := \prod_{i=1}^{N} P_i, \tag{3.1.2}$$

and the values of the parameters will be obtained by maximizing $\mathcal{L}(\mathbf{a})$.
In many applications, the natural logarithm of the likelihood function, called the log-likelihood, is more convenient to work with. Since the logarithm is a monotonically increasing function, the logarithm of a function achieves its maximum value at the same points as the function itself, and hence the log-likelihood can be used instead of the likelihood in maximum likelihood estimation and related techniques. Finding the maximum of a function often involves taking the derivative of the function and by solving for the parameter being maximized, this is often easier when the function being maximized is a log-likelihood rather than the original likelihood function. Therefore, we define

$$\mathcal{M} := \ln \mathcal{L} = \sum_{i=1}^{N} \ln P_i. \tag{3.1.3}$$

For example the logarithm of a product is a sum of individual logarithms, and the derivative of a sum of terms is often easier to compute than the derivative of a product. In addition, several common distributions have likelihood functions that contain products of factors involving exponentiation. The logarithm of such a function is a sum of products, making it simpler to differentiate than the original function.

3.2 Method of Least Squares

Another method to fit data is the least squares method. It is a standard approach in regression analysis to the solution. Its most important application is in data fitting. The best fit in the least-squares sense minimizes the sum of squared residuals, a residual being the difference between an observed value and the fitted value provided by a model.

Suppose that we have a data set (x_i, y_i) with $i = 1, 2, \ldots, N$. We know that $y = y(x)$ and we have a model

$$y = f(x, \mathbf{a}), \tag{3.2.1}$$

with $\mathbf{a} = [a_0, a_1, \ldots, a_{I-1}]$ the parameters of the model. Then, we want to find the values of the model parameters $\mathbf{a}$. To do that we can use the χ^2 function

$$\chi^2(\mathbf{a}) = \sum_{i=0}^{N-1} \left[\frac{y_i - f(x_i, \mathbf{a})}{\sigma_i} \right]^2, \tag{3.2.2}$$

with σ_i the error of the measurement y_i.
The best fit is the one that minimizes the sum of squared residuals, and this quantity is denoted $\chi^2_{\min}$. The gradient of χ^2 with respect to the parameters $\mathbf{a}$, which will be zero at the minimum of χ^2, has components

$$\frac{\partial \chi^2}{\partial a_k} = -2 \sum_{i=0}^{N-1} \frac{[y_i - f(x_i, \mathbf{a})]}{\sigma_i^2} \frac{\partial f(x_i, \mathbf{a})}{\partial a_k}, \tag{3.2.3}$$

with $k = 0, 1, 2, ..., I-1$. Taking an additional partial derivative of equation (3.2.3) gives

$$\frac{\partial^2 \chi^2}{\partial a_k \partial a_l} = 2 \sum_{i=0}^{N-1} \frac{1}{\sigma_i^2} \left[\frac{\partial f(x_i, \mathbf{a})}{\partial a_k} \frac{\partial f(x_i, \mathbf{a})}{\partial a_l} - [y_i - f(x_i, \mathbf{a})] \frac{\partial^2 f(x_i, \mathbf{a})}{\partial a_k \partial a_l} \right]. \tag{3.2.4}$$

It is conventional to remove the factors of 2 by defining

$$\beta_k := -\frac{1}{2} \frac{\partial \chi^2}{\partial a_k} \quad \text{(a)}, \qquad \alpha_{kl} := \frac{1}{2} \frac{\partial^2 \chi^2}{\partial a_k \partial a_l}. \quad \text{(b)} \tag{3.2.5}$$

On the other hand, the **Covariance Matrix** is defined as $C = \alpha^{-1}$ and

$$\sigma^2(a_i) := C_{ii}, \tag{3.2.6}$$

where $\sigma^2(a_i)$ is the variance of the a_i parameter (see chapter 15 of [39]).

It is important to mention that in case of a normal distribution error, the maximum likelihood method coincide with the least-squared method (see appendix section A.3.1).

3.3 Bayesian Analysis

In Statistics there are two "philosophies" about the interpretation of probability, the frequentist and the bayesian. In this thesis, we assume the Bayesian frame, where probability is interpreted as a *degree of belief* that something will happen, or that a parameter will have a given value.

Bayesian inference is a method of statistical inference in which Bayes's theorem is used to update the probability for a hypothesis as more evidence or information becomes available. Bayesian inference is an important technique in Statistics and it is particularly important in the dynamic analysis of a sequence of data. To compare different models of a certain physical phenomenon in light of the data there are criteria, based on the Occam's razor ("among competing hypotheses, the one with the fewest assumptions should be selected"). Let us quote a simple example from [40] which illustrates this rule. In Figure 3.1, it is observed the gray box and the white one behind it. One can postulate two models: first, there is one box behind the gray box, see Figure 3.2 left, second, there are two boxes of identical height and color behind the gray box, see Figure 3.2 right. Both models explain the observations equally well. According to Occam's principle we should accept the explanation which is simpler so that there is only one white box behind the gray one. Is it not more probable that there is only one box than two boxes with the same height and color? If we postulate that there are two boxes we need more parameters to describe this case than when there is just one box, for example we need to specify the width of the boxes.

Information criteria measure the goodness of fitted models compared to a base model (see [41]- [42]). Two widely used criteria are the Akaike Information Criterion (AIC) [43] and the Bayesian Information Criterion (BIC) [44]. The first is an essentially frequentist criterion based on information theory and the second one follows from an approximation for the bayesian evidence valid for large sample size [41].

In Cosmology AIC and BIC have been applied to discriminate cosmological models based on the penalization associated to the number of parameters that they need to explain the data. Specifically, in Ref. [45] the author perform cosmological model selection by using AIC and BIC in order to determinate the parameter set that better fit the WMAP3 data. Following this work in Ref. [13] the author considers more general models to the early Universe description in light of AIC and BIC, also including the deviance information criterion. Regarding late Universe description, the authors of Ref. [46] consider different models of dark energy and use information criteria to compare among them using the Gold sample of SN Ia. Later on, the authors of [47] study interacting models, with an energy density ratio proportional to a power-law of the scale factor attempting to alleviate the coincidence problem. By using AIC and BIC, they compare the models among themselves and with ΛCDM considering data from SN Ia, BAO and CMB.

More recently, in Ref. [13] the authors find that a particular interacting scenario is disfavored compared to ΛCDM. They study an interaction proportional to a power-law of the scale factor, by using AIC and BIC, and considering data from SnIa, H(z), BAO, Alcock-Paczynski test and CMB.

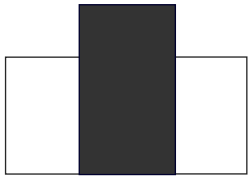

Figure 3.1: Illustration of a physical phenomenon observed. Source: Extracted from [13].

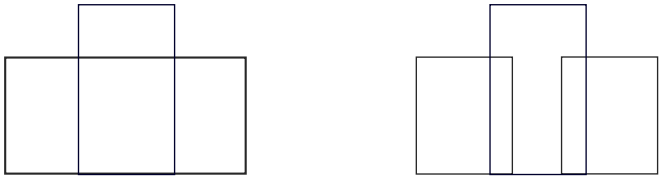

Figure 3.2: At left Hypothesis of one box and at right Hypotesis of two boxes. Source: Extracted from [13].

3.3.1 Akaike Information Criteria

In information theory there are no correct models, but only approximations to the reality, and these models depend on different parameters. The question then is to find which model would best approximate reality given the data we have recorded. In other words, we are trying to minimize the loss of information. Kullback and Leibler [48] addressed such issues and developed a measure, the Kullback-Leibler information, to represent the information lost when approximating reality (i.e., a good model minimizes the loss of information). A few decades later, Akaike [43] proposed using Kullback-Leibler information for model selection. He established a relationship between the maximum likelihood, and the Kullback-Leibler information. He developed an information criterion to estimate the Kullback-Leibler information, Akaike's information criterion (AIC) [43], which he described using a quantity defined as

$$\mathrm{AIC} = \chi^2_{\min} + 2d, \tag{3.3.1}$$

where d is the number of parameter of the model. Then, "the best model" according to this criterion is the one with a smaller value of AIC. We can note that this criterion "penalizes" models having a higher number of parameters.

For example, to compare the model H_i with the model H_j, we use $\Delta\mathrm{AIC}_{ij} = \mathrm{AIC}_i - \mathrm{AIC}_j$ that can be interpreted as "evidence in favour" of i model. Here AIC_j is a reference value of a test model. For $0 \leq \Delta\mathrm{AIC}_{ij} < 2$ we say that we have "strong evidence in favour" of model H_i, for $4 < \Delta\mathrm{AIC}_{ij} \leq 7$ there is "little evidence in favour" of the model H_i, and for $\Delta\mathrm{AIC}_{ij} > 10$ basically there is "no evidence in favour" of model H_i [13].

3.3.2 Bayesian Information Criteria

The bayesian approach to hypothesis testing was developed by Jeffreys [49]. Jeffreys was concerned with the comparison of predictions made by two competing scientific theories. In this approach, statistical models are introduced to represent the probability of the data according to each of the two theories. For this interpretation of model selection first we need to introduce the Bayes theorem. Let A and B be *events* with probabilities $pd(A)$ and $pd(B)$ ($pd(B) \neq 0$) respectively. Then the Bayes's theorem says that

$$pd(A|B) = \frac{pd(B|A)\, pd(A)}{pd(B)}, \tag{3.3.2}$$

where $pd(A|B)$, a conditional probability, is the probability of observing event A given that B is true and $pd(B|A)$ is the probability of observing event B given that A is true.

Thus, we begin with data $\mathbf{D}$, assumed to have arisen under one of the two hypotheses H_1 or H_2 according to a probability density $pd(\mathbf{D}|H_1)$ or $pd(\mathbf{D}|H_2)$, further we have a priori probabilities $pd(H_1)$ and $pd(H_2)$ such that $pd(H_2) = 1 - pd(H_1)$.

From Bayes theorem [49], we obtain

$$pd(H_k|\mathbf{D}) = \frac{pd(\mathbf{D}|H_k)pd(H_k)}{pd(\mathbf{D}|H_1)pd(H_1) + pd(\mathbf{D}|H_2)pd(H_2)}, \tag{3.3.3}$$

with $k = 1, 2$. Then, we can write

$$\frac{pd(H_1|\mathbf{D})}{pd(H_2|\mathbf{D})} = \frac{pd(\mathbf{D}|H_1)pd(H_1)}{pd(\mathbf{D}|H_2)pd(H_2)}. \tag{3.3.4}$$

Thus, in words,

$$\text{posterior odds} = (\text{Bayes factor}) \times (\text{prior odds}), \tag{3.3.5}$$

where the Bayes factor is defined by

$$B_{12} := \frac{pd(\mathbf{D}|H_1)}{pd(\mathbf{D}|H_2)}. \tag{3.3.6}$$

In other words, the Bayes factor is the ratio of the posterior odds of H_1 to its prior odds, regardless of the value of the prior odds. Thus, we can interpret the Bayes factor as a summary of the evidence provided by the data in favour of one scientific theory, represented by a statistical model, as opposed to another [50].

In general, it is very difficult to compute the Bayes factor, but we can write an approximation for it proposed by Schwarz [44] (conveniently defined in terms of the logarithm of the Bayes factor) as

$$\log B_{12} \approx \log pd(D|\dot{\mathbf{a}}_1, H_1) - \log pd(D|\dot{\mathbf{a}}_2, H_2) - (d_1 - d_2)\frac{1}{2}\log N, \tag{3.3.7}$$

where $\dot{\mathbf{a}}_k$ are the maximum likelihood parameters of the k model, d_k is the dimension of $\mathbf{a}$, and N is the sample size. Since, $\log pd(D|\dot{\mathbf{a}}_n, H_n)$ corresponds to the logarithm of the probability density, it coincides with the logarithm of the likelihood function, then defining (for a gaussian probability)

$$\text{BIC} := \chi^2_{\min} + d\ln N, \tag{3.3.8}$$

we get that

$$\log B_{12} = \text{BIC}_1 - \text{BIC}_2. \tag{3.3.9}$$

The Bayesian criterion was developed for the comparison of two models, but practical data analysis often involves far more than two models, at least implicitly. In this case, carrying out multiple frequentist tests to guide a search for the best model can give very misleading results. With regard to Bayesian calibration of frequentist methods, for large samples, the Bayesian criterion may be used to obtain the required value of an approximate t statistic[1] for it, to represent strong or decisive evidence [50]. Equation (3.3.6) can be rewritten (for large samples) as

$$\log B_{12} \approx t^2 - (d_1 - d_2)\log(N). \tag{3.3.10}$$

Assuming that $d_1 - d_2 = 1$, we can assign to the approximate t different degrees of "evidence". For "positive" evidence, this is $t = \sqrt{\log N}$, for "strong" evidence, it is $t = \sqrt{\log N + 6}$, and for "decisive" evidence, it is $t = \sqrt{\log N + 10}$.

Similarly to ΔAIC_{ij}, we define $\Delta\text{BIC}_{ij} = \text{BIC}_i - \text{BIC}_j$ which can be interpreted as "evidence" against the model i [13]. For $0 \leq \Delta\text{BIC}_{ij} < 2$ there is not enough evidence against the model, for $2 \leq \Delta\text{BIC}_{ij} < 6$ there is evidence against the model and for $6 \leq \Delta\text{BIC}_{ij} < 10$ there is strong evidence against model i.

[1] T statistic is used in order to find evidence of a significant difference between population means (2-sample t) or between the population mean and a hypothesized value (1-sample t). The t-value measures the size of the difference relative to the variation in your sample data.

Chapter 4

Analysis and Results

In this work we analyze eight general types of interacting models with analytical solution using supernovae type Ia (Constitution, Union, Union 2.1 and JLA), H(z) and BAO data, under the Akaike information criterion and the Bayesian information criterion. The main goal of our work is to investigate if complex interacting models are competitive in fitting the data and whether we could distinguish among them via a model comparison approach based on information criteria.

4.1 Theoretical Interactions

To analyze cosmological interaction using data at high redshift we need to include radiation in our calculations. When we consider radiation in the total energy density, i.e. $\rho = \rho_{\rm m} + \rho_{\rm x} + \rho_{\rm r}$, (2.4.5) is rewritten as

$$\rho_{\rm x} = \frac{\gamma_{\rm m}\varrho + \varrho'}{\Delta}, \qquad \rho_{\rm m} = -\frac{\gamma_{\rm x}\varrho + \varrho'}{\Delta}, \tag{4.1.1}$$

with $\varrho := \rho - \rho_{\rm r}$. The source equation (2.4.6) now is given by

$$\varrho'' + (\gamma_{\rm x} + \gamma_{\rm m})\varrho' + \gamma_{\rm x}\gamma_{\rm m}\varrho = \Delta\Gamma. \tag{4.1.2}$$

The solution (2.4.8) is valid for late time evolution, nevertheless if we are interested into consider data from BAO and/or CMB, which consider high redshifts, we need to take into account the radiation contribution in the equations. If we consider $\rho = \rho_{\rm m} + \rho_{\rm x} + \rho_{\rm r}$, with $\rho_{\rm r}$ the energy density of relativistic matter, which we assume it is non-interacting with the other fluids, the solution (2.4.8) of equation (2.4.7) is still valid but now, for interactions $\Gamma_1 - \Gamma_5$ we have

$$\rho(a) \;\; = \left[C_1 a^{\frac{3}{2}\lambda_1} + C_2 a^{\frac{3}{2}\lambda_2}\right]^{\frac{1}{1+b_2}} + 3H_0^2(1 - \Omega_{\rm x0} - \Omega_{\rm m0})a^{-4}, \tag{4.1.3}$$

where $\Omega_{\rm m0}$ is the density parameter of DM and baryons today, $\Omega_{\rm m0} = \Omega_{\rm b0} + \Omega_{\rm DM0}$ and the constants C_1 and C_2 are given by

$$C_1 = \left[3H_0^2(\Omega_{\rm x0} + \Omega_{\rm m0})\right]^{1+b_2} - C_2 \tag{4.1.4}$$

$$C_2 = -\left[3H_0^2(\Omega_{\rm x0} + \Omega_{\rm m0})\right]^{b_2}\left[3H_0^2(\Omega_{\rm x0}\gamma_{\rm x} + \Omega_{\rm m0}\gamma_{\rm m})\right](1 + b_2)/(\lambda_2 - \lambda_1) - \lambda_1\left[3H_0^2(\Omega_{\rm x0} + \Omega_{\rm m0})\right]^{1+b_2}/(\lambda_2 - \lambda_1) \tag{4.1.5}$$

The value of the constants b_1, b_2, b_3 is given in Table 2.2.

For interaction Γ_6 we can decompose the general solution into a homogeneous solution $\rho_{\rm h}$ and a particular solution $\rho_{\rm p}$, then the general solution is given by $\rho = \rho_{\rm h} + \rho_{\rm p}$. The homogeneous part of the solution $\rho_{\rm h}$ corresponds to (4.1.3) and the particular solution is given by:

$$\rho_{\rm p}(a) = -9Ra^{-4}, \tag{4.1.6}$$

where $R = 3\alpha\Delta H_0^2(1-\Omega_{\rm m0}-\Omega_{\rm x0})/(12b_1-9b_3-16)$ and the constants C_1 and C_2 are given by:

$$C_1 = 3H_0^2(\Omega_{\rm x0}+\Omega_{\rm m0})+9R-C_2, \tag{4.1.7}$$

$$C_2 = \frac{3H_0^2\Delta\Omega_{\rm x0}-(9\lambda_1+12)R-\left[3H_0^2(\Omega_{\rm x0}+\Omega_{\rm m0})\right](\gamma_{\rm m}+\lambda_1)}{\lambda_2-\lambda_1}. \tag{4.1.8}$$

For Γ_7 and Γ_8 we use the same method to find $\rho(a)$ where the homogeneous part $\rho_{\rm h}$ is given by (4.1.3) and the particular solution is (4.1.6), the constants C_1 and C_2 take the form of Eqs. (4.1.7) and (4.1.8) and for Γ_7 and Γ_8, $R = -4\alpha\Delta H_0^2(1-\Omega_{\rm m0}-\Omega_{\rm x0})/(12b_1-9b_3-16)$ and $R = -2\alpha\Delta H_0^2(1-\Omega_{\rm m0}-\Omega_{\rm x0})/(12b_1-9b_3-16)$ respectively.

We can therefore calculate the asymptotic limit of the coincidence parameter $r(a)$ in Eq. (2.4.14) when a tends to ∞. For all our interactions we get that

$$r_\infty = -\left[1+\frac{2(\gamma_{\rm x}-1)(1+b_2)}{2(1+b_2)-b_1+\sqrt{b_1^2-4b_3(1+b_2)}}\right], \tag{4.1.9}$$

a constant that depends on the state parameters and interaction parameters. The author of Ref. [18] noticed that for a constant and positive γ_x and for an interacting term proportional to ρ, ρ' or ρ_x, it is obtained a positive r parameter asymptotically constant, alleviating in this sense the coincidence problem.

4.2 Observational analysis

In our calculations we consider the energy density of radiation for photons and neutrinos, since the photons are accompanied with neutrinos and antineutrinos, giving a total energy density in radiation (that is, in massless or nearly massless particles) given by

$$\Omega_{\rm r0} = \left[1+N_{\rm eff}\left(\frac{7}{8}\right)\left(\frac{4}{11}\right)^{4/3}\right]\Omega_{\gamma 0}, \tag{4.2.1}$$

where $N_{\rm eff}$ is the effective number of types of neutrinos and $\Omega_{\gamma 0}$ is the energy density of photons whose value today is known from the CMB temperature $\Omega_{\gamma 0} = 2.469\times10^{-5}h^{-2}$ [1]. The deduction and calculus of (4.2.1) can be found in [1]. In this analysis it is considered the value of $N_{\rm eff} = 3.04$ according to [51].

It is also considered in this analysis the energy density of baryons $\Omega_{\rm b0} = 0.02222h^{-2}$ obtained from Planck Collaboration [3].

In order to analize the different interacting models, the following data is used: i) Distance modulus (μ) v/s redshift (z) of type Ia supernovae from the Constitution, Union 2 and Union 2.1 and binned JLA compilations, ii) $H(z)$ from ref. [52], iii) Acoustic parameter ($A(z)$, 3 data points from the WiggleZ experiment [53]) and the distance ratio, (d_z, 2 data points from the SDSS [54] and 1 data point from the 6dFGS [55] surveys), see below, obtained from the analysis of the baryonic acoustic oscillations.

In order to fit the cosmological models to the data the Chi-Square Method is used. Each data set (Constitution, Union 2, Union 2.1, $H(z)$, WiggleZ, SDSS and 6dFGS) has a corresponding Chi-Square function ($\chi^2_{\rm SN}$, $\chi^2_{\rm H}$, $\chi^2_{\rm WiggleZ}$, $\chi^2_{\rm SDSS}$ and $\chi^2_{\rm 6dFGS}$ respectively). For the Supernovae data we choose one of the three data sets and compute the corresponding Chi-Squared function $\chi^2_{\rm SN}$. We did not include CMB data in our analysis because the shift parameter is well defined only in the case of matter conservation [37], not in the case of interacting scenarios. The available data presented in Section 2.5.5 is given in terms of a covariance matrix, where the shift parameter and its error is already taken into account, then we can not use these data in our analysis.

Theses functions are defined as follows:

- For the type Ia Supernovae we use

$$\chi^2_{\rm SN} = \sum_{i=1}^{N} \frac{(\mu_{i,\rm th} - \mu_{i,\rm obs})^2}{\sigma_i^2}, \tag{4.2.2}$$

where $\mu(z)$ is the distance modulus, "th" represents the theoretical function, "obs" the observed value and σ_i is the error associated to the observed value.

- Similarly, for $H(z)$ we have,

$$\chi^2_{\rm H} = \sum_{i=1}^{N} \frac{(H_{i,\rm th} - H_{i,\rm obs})^2}{\sigma_i^2}. \tag{4.2.3}$$

- In the case of WiggleZ we use the inverse of the covariance matrix [53],

$$\chi^2_{\rm WiggleZ} = (A_{\rm th} - A_{\rm obs}) C^{-1}_{\rm WiggleZ} (A_{\rm th} - A_{\rm obs})^T, \tag{4.2.4}$$

with $A_{\rm obs} = (0.474, 0.442, 0.424)$ at redshifts $z = (0.44, 0.6, 0.73)$ respectively, and

$$C^{-1}_{\rm WiggleZ} = \begin{pmatrix} 1040.3 & -807.5 & 336.8 \\ -807.5 & 3720.3 & -1551.9 \\ 336.8 & -1551.9 & 2914.9 \end{pmatrix}. \tag{4.2.5}$$

- Analogously, for SDSS [54] we have

$$\chi^2_{\rm SDSS} = (d_{\rm th} - d_{\rm obs}) C^{-1}_{\rm SDSS} (d_{\rm th} - d_{\rm obs})^T, \tag{4.2.6}$$

with $d_{\rm obs} = (0.1905, 0.1097)$ at redshifts $z = (0.2, 0.35)$ and

$$C^{-1}_{\rm SDSS} = \begin{pmatrix} 30124 & 17227 \\ -17227 & 86977 \end{pmatrix}. \tag{4.2.7}$$

- Finally, for 6dRFGS, where we only have one data point, we define

$$\chi^2_{\rm 6dFGS} = \left(\frac{d_{\rm th} - d_{\rm obs}}{\sigma} \right)^2, \tag{4.2.8}$$

with $d_{\rm obs} = 0.336$ and $\sigma = 0.015$, at redshift $z = 0.106$ [55].

Then, each Chi-Squared function depends on the parameters of the models and in order to find the best fit model parameters we perform a joint analysis by using all the indicated data by minimizing the χ^2 function defined as:

$$\chi^2 = \chi^2_{\rm SN} + \chi^2_{\rm H(z)} + \chi^2_{\rm BAO}, \tag{4.2.9}$$

where $\chi^2_{\rm BAO} = \chi^2_{\rm WiggleZ} + \chi^2_{\rm SDSS} + \chi^2_{\rm 6dFGS}$.

4.3 Model fitting

For model fitting we use the Chi-Squared method through the Levenberg-Marquardt algorithm (see appendix, section A.5) implemented in the package lmfit of Python. For all the studied interactions we use a fixed $\gamma_{\rm m}$. The search ranges of the free parameters in our models are: $\Omega_{\rm m} \in [0,1]$, $\gamma_{\rm x} \in [-0.5, 0.5]$, $\alpha \in [-0.5, 0.5]$, $\beta \in [-0.5, 0.5]$ and $h \in [0,1]$. We use the combined datasets Union 2.1 (Constitution, Union 2 or JLA), $H(z)$ and BAO for the data fitting and we restrict our analysis to a maximum of 4 free parameters for each model.

We fix parameters such as $\gamma_{\rm m} = 1$ which corresponds to a cold dark matter scenario or $(\gamma_{\rm m}, \gamma_{\rm x}) = (1, 0)$ that corresponds to a $\Lambda(t)$CDM model [14]. For these scenarios we can additionally fix the parameters associated with different models of phenomenological interaction, α and/or β. Furthermore, in our analysis, we do not consider for interacting model Γ_2 the cases "a" ($\gamma_{\rm x}$ fixed to 0) and "f" ($\gamma_{\rm x}$ and α fixed to 0) since, for these 2 cases the uncertainty associated to the parameter estimation grows significantly.

In Table 4.1 the best fit parameters for all the analyzed models are shown, we used a joint analysis considering Union 2.1+H(z)+BAO. We have also included, besides interacting models, ΛCDM and ωCDM models as comparison. In this table all interacting scenarios and ωCDM model present a negative value of the barotropic index of DE (γ_x), indicating that there is a trend in favour of phantom DE models. Nevertheless, $\gamma_{\rm x}$ is compatible with zero considering the 1σ confidence level.

In Table 4.2 we show the joint analysis considering only Union 2.1 and H(z) data, for the studied models with three free parameters. We note that all the results are consistent in general with the results in Table 4.1 but the uncertainty associated to the interaction parameters α and β are larger when we use only these data. Furthermore, in Table 4.1 the sign of the interaction parameters can be positive or negative in most of these cases inside the 1σ region for the parameter. By considering only Union 2.1 and H(z) data we restrict ourselves to three free parameters because, in order to constrain models with more parameters we would need more data. For instance, we notice that in models of four free parameters the confidence interval became significantly large in comparison with models of three free parameters. This degeneracy decreases when we add BAO data to the joint analysis.

In Tables 4.1 and 4.2 we noticed that even though there is a deviation from the ΛCDM scenario, we obtained similar values for the current deceleration parameter q_0, the current effective state parameter $\omega_{\rm eff}$ and the age of our Universe for all the studied interacting scenarios.

In Table 4.3 we extend our analysis by considering binned data of the more recent JLA compilation of SN Ia [26]. We note that for the joint analysis using Union 2.1 or JLA compilation the results are consistent, and in light of the Bayesian information criterion, the interacting models are ordered according to the number of free parameters of each model.

In our analysis ΛCDM is the model with the lowest BIC parameters when we use data from the joint analysis of Union2.1+H(z)+BAO (Table 4.1), Union2.1+H(z) (Table 4.2) or JLA+H(z)+BAO (Table 4.3). From Figure 4.1 we see that, when the underlying model is assumed to be ΛCDM, AIC indicates that all models with 3 free parameters are in the region of "strong evidence in favor". Nevertheless under BIC, interacting models with 4 free parameters are further than having "strong evidence against" and the models of 3 free parameters are in the upper limit of having "evidence against". The model ωCDM is also incompatible with ΛCDM with respect to BIC. From Figures 4.1 and 4.2, we notice a tension between AIC and BIC results, while AIC indicates there is "evidence in favor" BIC indicates that there is "evidence against" or "strong evidence against" for the same model. This is due to the fact that BIC strongly penalizes models when they have a larger number of parameters [45].

Regarding BIC, there are not interacting models compatible with ΛCDM in our work. This is consistent with the results of Ref. [13], where the authors conclude that the particular interacting model they study is disfavored compared to ΛCDM, also they notice that BIC is a more stringent criteria. From here on we restrict ourselves to the more stringent criteria. According to BIC the models are ordered in agreement with the number of free parameters, as we see in Table 4.3.

If we compare the models without considering ΛCDM, the best model according to AIC and

Model	$\Omega_{\rm m}$	$\gamma_{\rm x}$	α	β	h	q_0	$\omega_{\rm eff}$	Age	AIC	BIC
Γ_{1a}	0.243 ± 0.026	Fixed	0.005 ± 0.009	-0.03 ± 0.070	0.699 ± 0.003	-0.567 ± 0.040	-0.711 ± 0.026	13.786 ± 0.684	587.789	605.469
Γ_{1b}	0.247 ± 1.495	-0.059 ± 2.211	Fixed	0.005 ± 2.266	0.701 ± 0.004	-0.624 ± 3.339	-0.75 ± 2.226	13.614 ± 25.424	587.423	605.103
Γ_{1c}	0.246 ± 0.044	-0.053 ± 0.134	0.001 ± 0.011	Fixed	0.701 ± 0.004	-0.618 ± 0.158	-0.746 ± 0.105	13.637 ± 0.653	587.398	605.078
Γ_{1d}	0.246 ± 0.049	-0.053 ± 0.140	0.001 ± 0.011	0.001 ± 0.011	0.701 ± 0.004	-0.619 ± 0.167	-0.746 ± 0.111	13.633 ± 0.722	587.400	605.080
Γ_{1e}	0.238 ± 0.022	Fixed	Fixed	0.005 ± 0.052	0.699 ± 0.003	-0.574 ± 0.033	-0.716 ± 0.022	13.652 ± 0.475	586.500	599.760
Γ_{1f}	0.235 ± 0.015	Fixed	0.003 ± 0.008	Fixed	0.699 ± 0.003	-0.579 ± 0.022	-0.719 ± 0.015	13.687 ± 0.219	586.049	599.309
Γ_{2b}	0.247 ± 1.712	-0.059 ± 2.531	Fixed	0.079 ± 40.317	0.701 ± 0.004	-0.625 ± 3.824	-0.750 ± 2.550	13.613 ± 29.852	587.423	605.103
Γ_{2c}	0.246 ± 0.044	-0.052 ± 0.134	-0.001 ± 0.011	Fixed	0.701 ± 0.004	-0.618 ± 0.158	-0.746 ± 0.106	13.637 ± 0.656	587.398	605.078
Γ_{2d}	0.246 ± 0.044	-0.053 ± 0.134	-0.001 ± 0.011	-0.001 ± 0.011	0.701 ± 0.004	-0.619 ± 0.158	-0.746 ± 0.106	13.636 ± 0.656	587.398	605.078
Γ_{2e}	0.235 ± 0.015	Fixed	-0.003 ± 0.008	Fixed	0.699 ± 0.003	-0.579 ± 0.022	-0.719 ± 0.015	13.687 ± 0.219	586.049	599.309
Γ_{3}	0.246 ± 0.042	-0.052 ± 0.132	0.001 ± 0.006	– – –	0.701 ± 0.004	-0.618 ± 0.156	-0.746 ± 0.104	13.637 ± 0.638	587.398	605.078
Γ_{3a}	0.235 ± 0.015	Fixed	0.002 ± 0.004	– – –	0.699 ± 0.003	-0.579 ± 0.022	-0.719 ± 0.015	13.690 ± 0.214	586.040	599.300
Γ_{4}	0.246 ± 0.042	-0.052 ± 0.132	0.001 ± 0.011	– – –	0.701 ± 0.004	-0.618 ± 0.155	-0.745 ± 0.103	13.638 ± 0.627	587.398	605.078
Γ_{4a}	0.235 ± 0.014	Fixed	0.003 ± 0.008	– – –	0.699 ± 0.003	-0.579 ± 0.022	-0.719 ± 0.014	13.693 ± 0.208	586.032	599.292
Γ_{5}	0.248 ± 0.157	-0.060 ± 0.206	0.006 ± 0.455	– – –	0.701 ± 0.004	-0.624 ± 0.331	-0.749 ± 0.221	13.618 ± 2.685	587.430	605.110
Γ_{5a}	0.241 ± 0.024	Fixed	-0.006 ± 0.095	– – –	0.699 ± 0.003	-0.570 ± 0.035	-0.713 ± 0.024	13.672 ± 0.499	586.507	599.767
Γ_{6}	0.246 ± 0.047	-0.053 ± 0.138	0.001 ± 0.010	– – –	0.701 ± 0.004	-0.619 ± 0.164	-0.746 ± 0.110	13.634 ± 0.713	587.400	605.080
Γ_{6a}	0.235 ± 0.015	Fixed	0.003 ± 0.007	– – –	0.699 ± 0.003	-0.580 ± 0.023	-0.720 ± 0.015	13.679 ± 0.243	586.094	599.354
Γ_{7}	0.246 ± 0.043	-0.053 ± 0.133	-0.001 ± 0.010	– – –	0.701 ± 0.004	-0.619 ± 0.156	-0.746 ± 0.104	13.637 ± 0.642	587.398	605.078
Γ_{7a}	0.235 ± 0.015	Fixed	-0.003 ± 0.007	– – –	0.699 ± 0.003	-0.579 ± 0.022	-0.719 ± 0.015	13.690 ± 0.216	586.046	599.306
Γ_{8}	0.247 ± 0.034	-0.050 ± 0.122	0.003 ± 0.025	– – –	0.701 ± 0.004	-0.616 ± 0.140	-0.744 ± 0.093	13.647 ± 0.528	587.394	605.074
Γ_{8a}	0.237 ± 0.013	Fixed	0.010 ± 0.021	– – –	0.699 ± 0.003	-0.576 ± 0.020	-0.718 ± 0.013	13.717 ± 0.198	585.915	599.175
ωCDM	0.249 ± 0.027	-0.059 ± 0.093	– – –	– – –	0.701 ± 0.004	-0.622 ± 0.107	-0.748 ± 0.072	13.625 ± 0.409	585.435	598.695
ΛCDM	0.240 ± 0.014	– – –	– – –	– – –	0.699 ± 0.003	-0.571 ± 0.021	-0.714 ± 0.014	13.665 ± 0.189	584.513	593.353

Table 4.1: Results of the data fitting using the joint analysis from Union 2.1, $H(z)$ and BAO. The error informed corresponds to 68% confidence level. Fixed means that the parameter was set to zero and the dashed lines mean that the model do not have that parameter. q_0 is the current value of the deceleration parameter, $w_{\rm eff}$ is the value of the effective state parameter today and it is reported the calculated age of the Universe in Gy. The AIC and BIC parameters are indicated in each case. The uncertainties associated to the parameter q_0, $w_{\rm eff}$ and the age of the Universe were calculated using propagation of uncertainty (see appendix, section A.4). Source: Own elaboration.

Model	$\Omega_{\rm m}$	$\gamma_{\rm x}$	α	β	h	q_0	$\omega_{\rm eff}$	Age	AIC	BIC
Γ_{1d}	0.214 ± 0.055	Fixed	Fixed	0.047 ± 0.129	0.701 ± 0.004	-0.613 ± 0.082	-0.742 ± 0.055	13.65 ± 1.149	583.985	597.215
Γ_{1e}	0.218 ± 0.032	Fixed	0.054 ± 0.109	Fixed	0.701 ± 0.004	-0.607 ± 0.049	-0.738 ± 0.032	13.42 ± 1.106	583.889	597.119
Γ_{2d}	0.218 ± 0.032	Fixed	-0.052 ± 0.098	Fixed	0.701 ± 0.004	-0.607 ± 0.049	-0.738 ± 0.032	13.420 ± 1.106	583.889	597.119
Γ_{3a}	0.220 ± 0.030	Fixed	0.035 ± 0.068	– – –	0.701 ± 0.004	-0.605 ± 0.045	-0.737 ± 0.030	13.368 ± 1.141	583.880	597.110
Γ_{4a}	0.222 ± 0.026	Fixed	0.095 ± 0.178	– – –	0.701 ± 0.004	-0.602 ± 0.038	-0.734 ± 0.026	13.280 ± 1.205	583.867	597.098
Γ_{5a}	0.214 ± 0.066	Fixed	0.073 ± 0.248	– – –	0.701 ± 0.004	-0.613 ± 0.099	-0.742 ± 0.066	13.686 ± 1.280	584.028	597.259
Γ_{6a}	0.215 ± 0.043	Fixed	0.026 ± 0.060	– – –	0.701 ± 0.004	-0.612 ± 0.065	-0.741 ± 0.043	13.534 ± 1.133	583.933	597.164
Γ_{7a}	0.218 ± 0.032	Fixed	-0.054 ± 0.109	– – –	0.701 ± 0.004	-0.607 ± 0.049	-0.738 ± 0.032	13.420 ± 1.106	583.889	597.119
Γ_{8a}	0.219 ± 0.076	Fixed	-0.051 ± 0.273	– – –	0.701 ± 0.005	-0.606 ± 0.114	-0.737 ± 0.076	13.799 ± 1.167	584.077	597.307
ωCDM	0.247 ± 0.041	-0.047 ± 0.129	– – –	– – –	0.701 ± 0.004	-0.613 ± 0.152	-0.742 ± 0.101	13.650 ± 0.607	583.985	597.215
ΛCDM	0.233 ± 0.016	– – –	– – –	– – –	0.700 ± 0.003	-0.585 ± 0.023	-0.723 ± 0.016	13.758 ± 0.222	582.118	590.938

Table 4.2: Results of the data fitting using the joint analysis from Union 2.1 and $H(z)$. Source: Own elaboration.

Model	BIC	f.p.	Model	BIC	f.p.
ΛCDM	58.489	2	ΛCDM	593.353	2
ωCDM	62.173	3	ωCDM	598.695	3
Γ_{8a}	62.231	3	Γ_{8a}	599.175	3
Γ_{4a}	62.329	3	Γ_{4a}	599.292	3
Γ_{3a}	62.337	3	Γ_{3a}	599.300	3
Γ_{7a}	62.342	3	Γ_{7a}	599.306	3
Γ_{1f}	62.345	3	Γ_{1f}	599.309	3
Γ_{6a}	62.381	3	Γ_{2e}	599.309	3
Γ_{5a}	62.654	3	Γ_{6a}	599.354	3
Γ_{1e}	62.661	3	Γ_{1e}	599.760	3
Γ_{2e}	62.664	3	Γ_{5a}	599.767	3
Γ_8	66.241	4	Γ_8	605.074	4
Γ_{1a}	66.245	4	Γ_{1c}	605.078	4
Γ_4	66.266	4	Γ_{2c}	605.078	4
Γ_3	66.268	4	Γ_{2d}	605.078	4
Γ_7	66.269	4	Γ_3	605.078	4
Γ_{1c}	66.270	4	Γ_4	605.078	4
Γ_{2c}	66.270	4	Γ_7	605.078	4
Γ_{2d}	66.270	4	Γ_{1d}	605.080	4
Γ_6	66.278	4	Γ_6	605.080	4
Γ_{1d}	66.279	4	Γ_{1b}	605.103	4
Γ_{1b}	66.342	4	Γ_{2b}	605.103	4
Γ_{2b}	66.342	4	Γ_5	605.110	4
Γ_5	66.347	4	Γ_{1a}	605.469	4

Table 4.3: Ranking of models according to BIC. In the left panel we show the joint analysis of binned JLA+$H(z)$+BAO and in the right panel we have the joint analysis of Union 2.1+$H(z)$+BAO. f.p. means number of free parameters in the model. Source: Own elaboration.

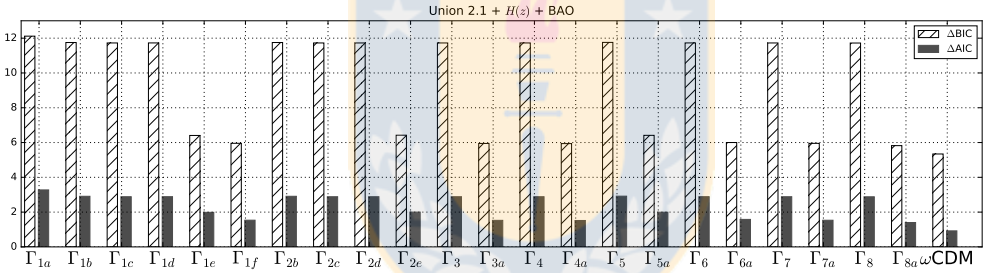

Figure 4.1: ΔAIC and ΔBIC of models defined in Table 4.1 compared to ΛCDM. Source: Own elaboration.

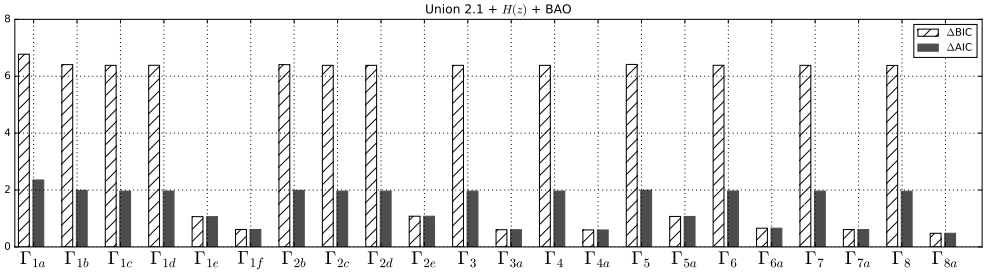

Figure 4.2: Models defined in Table 4.1 compared to the ωCDM model. Source: Own elaboration.

BIC is ωCDM. We note that under BIC all models with three free parameters (f.p.) can not be rule out when we assume that ωCDM is the underlying model, see Table 4.3. In Figure 4.2 we see that by using BIC there is "strong evidence against" models with 4 f.p. when the base model is ωCDM. We can rule out models of 4 f.p. but not models of 3 f.p. if the best model is

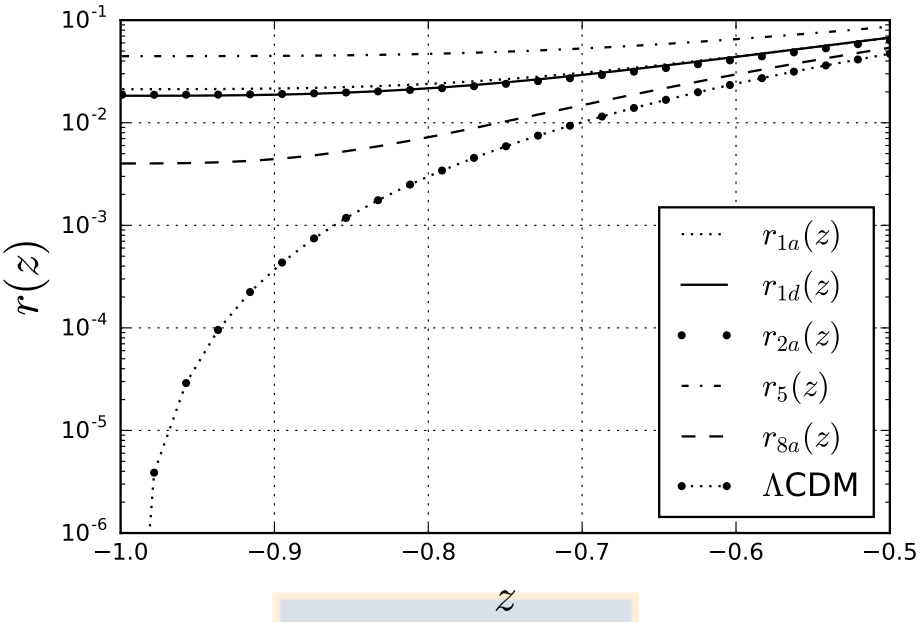

Figure 4.3: Coincidence parameter in semilog scale. By using Union 2.1 $+H(z)$+BAO, these interactions have an energy transfer from DE to DM today. Source: Own elaboration.

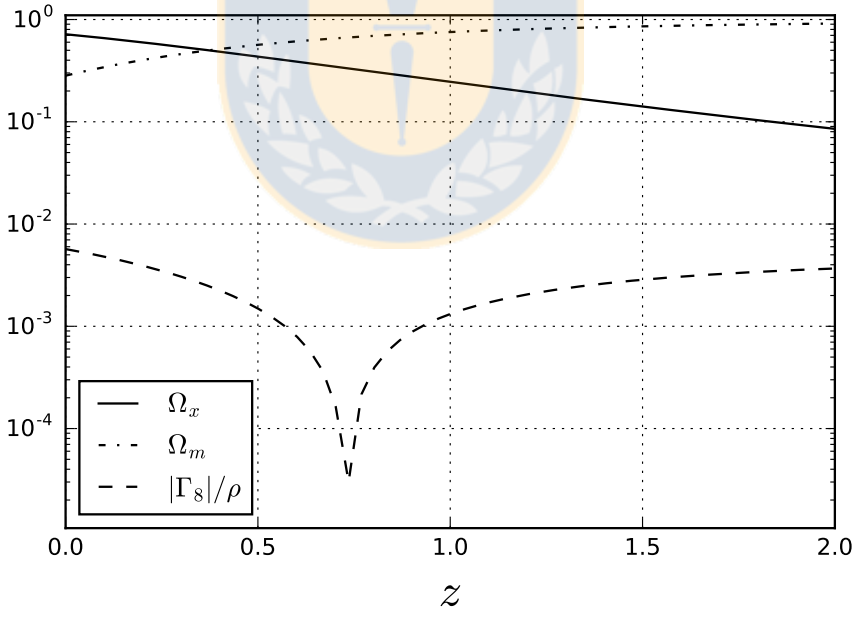

Figure 4.4: Semilog graphic of the evolution of the density parameters for the interacting model Γ_{8a} considering Union 2.1 $+H(z)$+BAO. Note that the interaction has a sign change at redshift $z = 0.7$ approximately. Source: Own elaboration.

ωCDM. On the other hand, the best interacting model under BIC (and AIC) is Γ_{8a}, which has an interaction proportional to the deceleration parameter q.

Among all our models, those shown in Figure 4.3 alleviate the coincidence problem, besides,

Model	$\Omega_{\rm m}$	$\gamma_{\rm x}$	α	β	h	q_0	$\omega_{\rm eff}$	Age	AIC	BIC
Γ_{1a}	0.248 ± 0.033	Fixed	-0.011 ± 0.013	0.048 ± 0.096	0.650 ± 0.004	-0.548 ± 0.05	-0.699 ± 0.033	14.264 ± 0.73	499.809	516.074
Γ_{1b}	0.251 ± 0.283	0.039 ± 0.389	Fixed	-0.025 ± 0.400	0.650 ± 0.005	-0.503 ± 0.575	-0.669 ± 0.383	14.544 ± 5.127	501.484	517.749
Γ_{1c}	0.260 ± 0.027	-0.003 ± 0.085	-0.007 ± 0.010	Fixed	0.650 ± 0.005	-0.534 ± 0.097	-0.689 ± 0.064	14.400 ± 0.426	500.290	516.555
Γ_{1d}	0.260 ± 0.028	0.003 ± 0.083	-0.006 ± 0.009	-0.006 ± 0.009	0.650 ± 0.005	-0.528 ± 0.095	-0.686 ± 0.063	14.424 ± 0.436	500.425	516.689
Γ_{1e}	0.256 ± 0.028	Fixed	Fixed	-0.024 ± 0.062	0.651 ± 0.004	-0.537 ± 0.042	-0.691 ± 0.028	14.511 ± 0.614	499.898	512.096
Γ_{1f}	0.259 ± 0.019	Fixed	-0.007 ± 0.010	Fixed	0.650 ± 0.004	-0.532 ± 0.029	-0.688 ± 0.019	14.403 ± 0.283	498.292	510.490
Γ_{2b}	0.251 ± 0.267	0.039 ± 0.368	Fixed	0.390 ± 5.620	0.650 ± 0.005	-0.503 ± 0.544	-0.669 ± 0.363	14.544 ± 6.024	501.484	517.749
Γ_{2c}	0.260 ± 0.027	-0.003 ± 0.085	0.007 ± 0.010	Fixed	0.650 ± 0.005	-0.534 ± 0.097	-0.689 ± 0.064	14.400 ± 0.425	500.290	516.555
Γ_{2d}	0.260 ± 0.027	-0.003 ± 0.085	0.007 ± 0.010	0.007 ± 0.010	0.650 ± 0.005	-0.534 ± 0.097	-0.69 ± 0.064	14.400 ± 0.422	500.290	516.554
Γ_{2e}	0.259 ± 0.019	Fixed	Fixed	0.999 ± 0.002	0.650 ± 0.004	-0.532 ± 0.029	-0.688 ± 0.019	14.404 ± 0.286	498.292	510.490
Γ_3	0.260 ± 0.027	-0.004 ± 0.085	-0.004 ± 0.006	$- - -$	0.650 ± 0.005	-0.535 ± 0.097	-0.690 ± 0.065	14.393 ± 0.415	500.252	516.517
Γ_{3a}	0.259 ± 0.019	Fixed	-0.004 ± 0.005	$- - -$	0.650 ± 0.004	-0.532 ± 0.029	-0.688 ± 0.019	14.397 ± 0.276	498.256	510.454
Γ_4	0.260 ± 0.027	-0.005 ± 0.086	-0.008 ± 0.011	$- - -$	0.650 ± 0.005	-0.537 ± 0.097	-0.691 ± 0.065	14.386 ± 0.416	500.213	516.478
Γ_{4a}	0.259 ± 0.019	Fixed	-0.007 ± 0.011	$- - -$	0.650 ± 0.004	-0.533 ± 0.029	-0.688 ± 0.019	14.390 ± 0.270	498.219	510.417
Γ_5	0.250 ± 0.088	0.043 ± 0.120	-0.044 ± 0.257	$- - -$	0.650 ± 0.005	-0.501 ± 0.179	-0.667 ± 0.119	14.538 ± 1.704	501.541	517.806
Γ_{5a}	0.254 ± 0.032	Fixed	-0.031 ± 0.129	$- - -$	0.652 ± 0.004	-0.541 ± 0.048	-0.694 ± 0.032	14.488 ± 0.685	500.020	512.219
Γ_6	0.260 ± 0.028	0.002 ± 0.083	-0.006 ± 0.008	$- - -$	0.650 ± 0.005	-0.529 ± 0.095	-0.686 ± 0.063	14.417 ± 0.443	500.392	516.656
Γ_{6a}	0.260 ± 0.020	Fixed	-0.006 ± 0.008	$- - -$	0.650 ± 0.004	-0.531 ± 0.030	-0.687 ± 0.020	14.415 ± 0.308	498.392	510.591
Γ_7	0.260 ± 0.027	-0.004 ± 0.085	0.006 ± 0.009	$- - -$	0.650 ± 0.005	-0.535 ± 0.097	-0.690 ± 0.064	14.391 ± 0.417	500.262	516.526
Γ_{7a}	0.259 ± 0.019	Fixed	0.006 ± 0.008	$- - -$	0.650 ± 0.004	-0.532 ± 0.029	-0.688 ± 0.019	14.395 ± 0.277	498.265	510.463
Γ_8	0.259 ± 0.026	-0.022 ± 0.095	-0.024 ± 0.032	$- - -$	0.651 ± 0.005	-0.555 ± 0.106	-0.703 ± 0.071	14.327 ± 0.388	499.922	516.186
Γ_{8a}	0.255 ± 0.019	Fixed	-0.021 ± 0.030	$- - -$	0.650 ± 0.004	-0.538 ± 0.029	-0.692 ± 0.019	14.352 ± 0.257	498.000	510.198
ωCDM	0.243 ± 0.021	0.036 ± 0.071	$- - -$	$- - -$	0.650 ± 0.005	-0.519 ± 0.081	-0.679 ± 0.054	14.469 ± 0.346	499.777	511.976
ΛCDM	0.248 ± 0.018	$- - -$	$- - -$	$- - -$	0.652 ± 0.004	-0.550 ± 0.027	-0.700 ± 0.018	14.445 ± 0.251	498.130	506.262

Table 4.4: Results of the data fitting using the joint analysis from Constitution, $H(z)$ and BAO. Source: Own elaboration.

Model	$\Omega_{\rm m}$	$\gamma_{\rm x}$	α	β	h	q_0	$\omega_{\rm eff}$	Age	AIC	BIC
Γ_{1a}	0.240 ± 0.024	Fixed	0.006 ± 0.009	-0.030 ± 0.065	0.699 ± 0.003	-0.572 ± 0.036	-0.715 ± 0.024	13.84 ± 0.648	568.383	585.910
Γ_{1b}	0.245 ± 1.916	-0.073 ± 2.861	Fixed	0.008 ± 2.935	0.702 ± 0.004	-0.643 ± 4.336	-0.762 ± 2.89	13.645 ± 32.835	567.587	585.114
Γ_{1c}	0.246 ± 0.043	-0.068 ± 0.135	0.001 ± 0.011	Fixed	0.701 ± 0.004	-0.636 ± 0.159	-0.757 ± 0.106	13.674 ± 0.655	567.590	585.118
Γ_{1d}	0.246 ± 0.049	-0.068 ± 0.144	0.001 ± 0.011	0.001 ± 0.011	0.702 ± 0.004	-0.636 ± 0.173	-0.758 ± 0.115	13.671 ± 0.741	567.589	585.116
Γ_{1e}	0.235 ± 0.022	Fixed	Fixed	0.007 ± 0.051	0.698 ± 0.003	-0.579 ± 0.033	-0.719 ± 0.022	13.692 ± 0.475	567.189	580.335
Γ_{1f}	0.232 ± 0.015	Fixed	0.004 ± 0.008	Fixed	0.699 ± 0.003	-0.584 ± 0.023	-0.723 ± 0.015	13.736 ± 0.227	566.648	579.793
Γ_{2b}	0.245 ± 2.091	-0.074 ± 3.123	Fixed	0.096 ± 39.266	0.702 ± 0.004	-0.643 ± 4.733	-0.762 ± 3.155	13.645 ± 37.018	567.587	585.114
Γ_{2c}	0.246 ± 0.044	-0.068 ± 0.136	-0.001 ± 0.011	Fixed	0.701 ± 0.004	-0.636 ± 0.160	-0.757 ± 0.107	13.673 ± 0.660	567.590	585.118
Γ_{2d}	0.246 ± 0.043	-0.068 ± 0.135	-0.001 ± 0.011	-0.001 ± 0.011	0.701 ± 0.004	-0.636 ± 0.159	-0.757 ± 0.106	13.674 ± 0.653	567.590	585.118
Γ_{2e}	0.232 ± 0.015	Fixed	-0.004 ± 0.008	Fixed	0.699 ± 0.003	-0.584 ± 0.023	-0.723 ± 0.015	13.736 ± 0.227	566.648	579.793
Γ_3	0.246 ± 0.042	-0.068 ± 0.132	0.000 ± 0.006	$- - -$	0.701 ± 0.004	-0.636 ± 0.156	-0.757 ± 0.104	13.675 ± 0.633	567.591	585.118
Γ_{3a}	0.232 ± 0.015	Fixed	0.002 ± 0.004	$- - -$	0.699 ± 0.003	-0.584 ± 0.022	-0.722 ± 0.015	13.739 ± 0.221	566.639	579.785
Γ_4	0.246 ± 0.041	-0.068 ± 0.132	0.001 ± 0.011	$- - -$	0.701 ± 0.004	-0.636 ± 0.155	-0.757 ± 0.103	13.674 ± 0.622	567.592	585.119
Γ_{4a}	0.232 ± 0.015	Fixed	0.004 ± 0.008	$- - -$	0.699 ± 0.003	-0.583 ± 0.022	-0.722 ± 0.015	13.742 ± 0.216	566.631	579.776
Γ_5	0.246 ± 0.146	-0.075 ± 0.195	0.011 ± 0.428	$- - -$	0.702 ± 0.004	-0.643 ± 0.313	-0.762 ± 0.209	13.650 ± 2.518	567.599	585.127
Γ_{5a}	0.239 ± 0.023	Fixed	-0.004 ± 0.092	$- - -$	0.698 ± 0.003	-0.574 ± 0.035	-0.716 ± 0.023	13.714 ± 0.492	567.212	580.358
Γ_6	0.246 ± 0.048	-0.068 ± 0.143	0.001 ± 0.010	$- - -$	0.701 ± 0.004	-0.636 ± 0.171	-0.758 ± 0.114	13.672 ± 0.736	567.589	585.117
Γ_{6a}	0.232 ± 0.016	Fixed	0.003 ± 0.007	$- - -$	0.699 ± 0.003	-0.584 ± 0.024	-0.723 ± 0.016	13.727 ± 0.251	566.700	579.845
Γ_7	0.246 ± 0.042	-0.068 ± 0.134	-0.001 ± 0.010	$- - -$	0.701 ± 0.004	-0.636 ± 0.158	-0.757 ± 0.105	13.674 ± 0.644	567.591	585.118
Γ_{7a}	0.232 ± 0.015	Fixed	-0.003 ± 0.007	$- - -$	0.699 ± 0.003	-0.584 ± 0.022	-0.722 ± 0.015	13.739 ± 0.223	566.646	579.791
Γ_8	0.246 ± 0.032	-0.067 ± 0.117	0.002 ± 0.025	$- - -$	0.701 ± 0.004	-0.634 ± 0.134	-0.756 ± 0.089	13.679 ± 0.500	567.595	585.123
Γ_{8a}	0.234 ± 0.014	Fixed	0.011 ± 0.021	$- - -$	0.699 ± 0.003	-0.581 ± 0.020	-0.721 ± 0.014	13.771 ± 0.206	566.496	579.642
ωCDM	0.248 ± 0.025	-0.073 ± 0.088	$- - -$	$- - -$	0.702 ± 0.004	-0.638 ± 0.102	-0.759 ± 0.068	13.664 ± 0.383	565.616	578.761
ΛCDM	0.238 ± 0.014	$- - -$	$- - -$	$- - -$	0.698 ± 0.003	-0.575 ± 0.021	-0.717 ± 0.014	13.708 ± 0.195	565.215	573.979

Table 4.5: Results of the data fitting using the joint analysis from Union 2, $H(z)$ and BAO. Source: Own elaboration.

all of them have an energy transfer from DE to DM today. In the case of Γ_{8a}, for $z > 0.7$ we have an energy transfer from DM to DE and for $z < 0.7$ the energy transfer is from DE to DM as we see in Figure 4.4.

It is noteworthy to mention that interaction Γ_{8a} is marginally better than other interacting models according to AIC and BIC and this interaction alleviates the coincidence problem and changes sign during evolution. A similar behavior was reported in Ref. [12] where the authors separate the data in redshift bins for $Q = 3H\delta$, where δ is a constant fitted for each bin. The authors consider different parameterizations of the equation of state for DE and they found an oscillation of the interaction sign. Sign-changeable interactions were also studied in Refs. [16,56]

As summary, from our analysis we notice that there are consistent interacting models that explain the data equally well that ωCDM, and an increase of the number of free parameters in interacting models is strongly penalized according to BIC in the description of the late Universe.

In Table 4.4, we consider data from Constitution, $H(z)$ and BAO, the "best interacting model" according to BIC is Γ_{8a} . Nevertheless, from these data we obtain that the parameter of state of DE $\gamma_{\rm x}$ for the different interactions changes sign (on the contrary of Union 2.1, $H(z)$

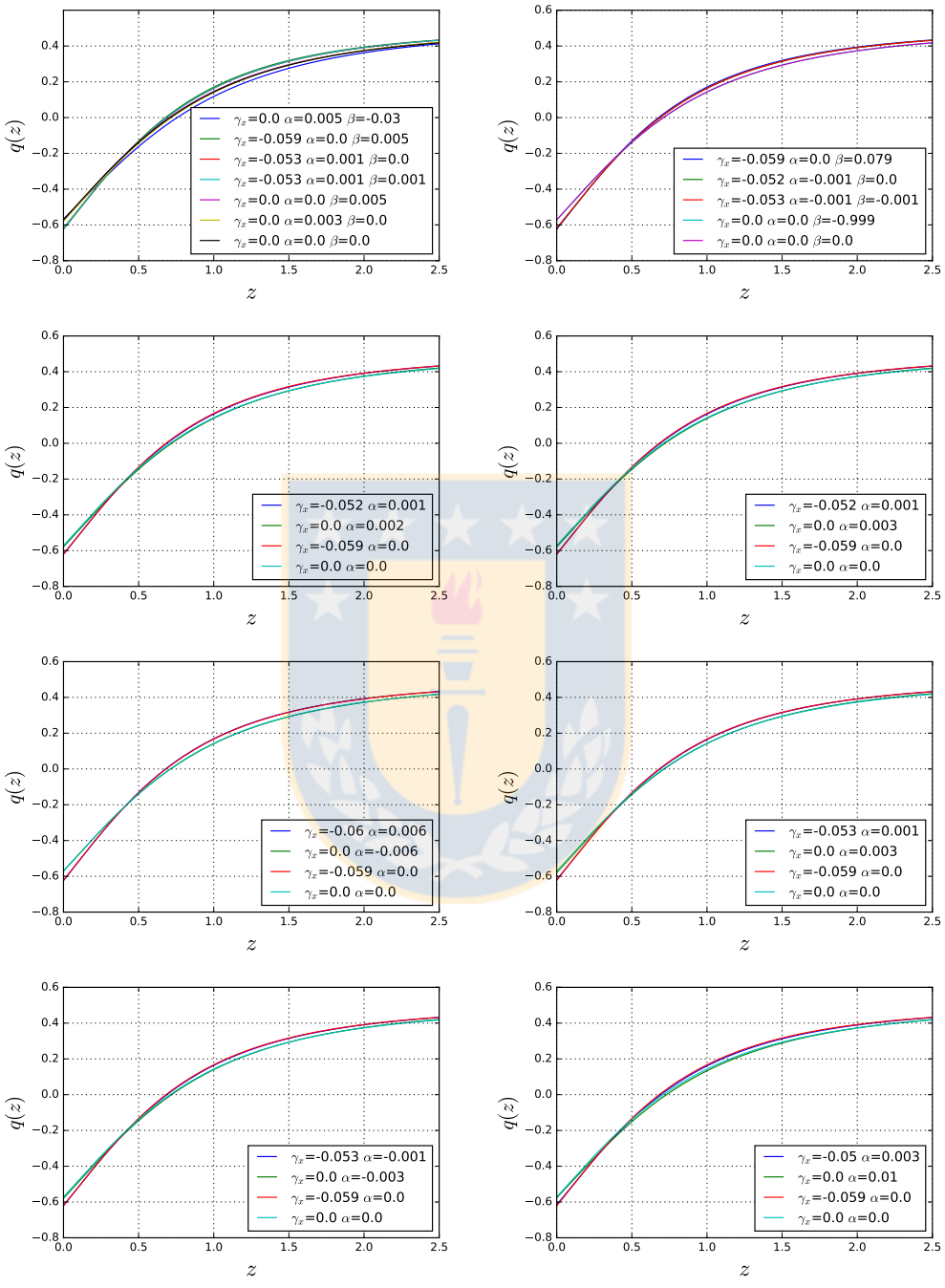

Figure 4.5: Deceleration parameter considering data from Union 2.1, $H(z)$ and BAO. The graphics are ordered by the number of interaction, from Γ_1 to Γ_8, from left to right and from top to bottom. Source: Own elaboration.

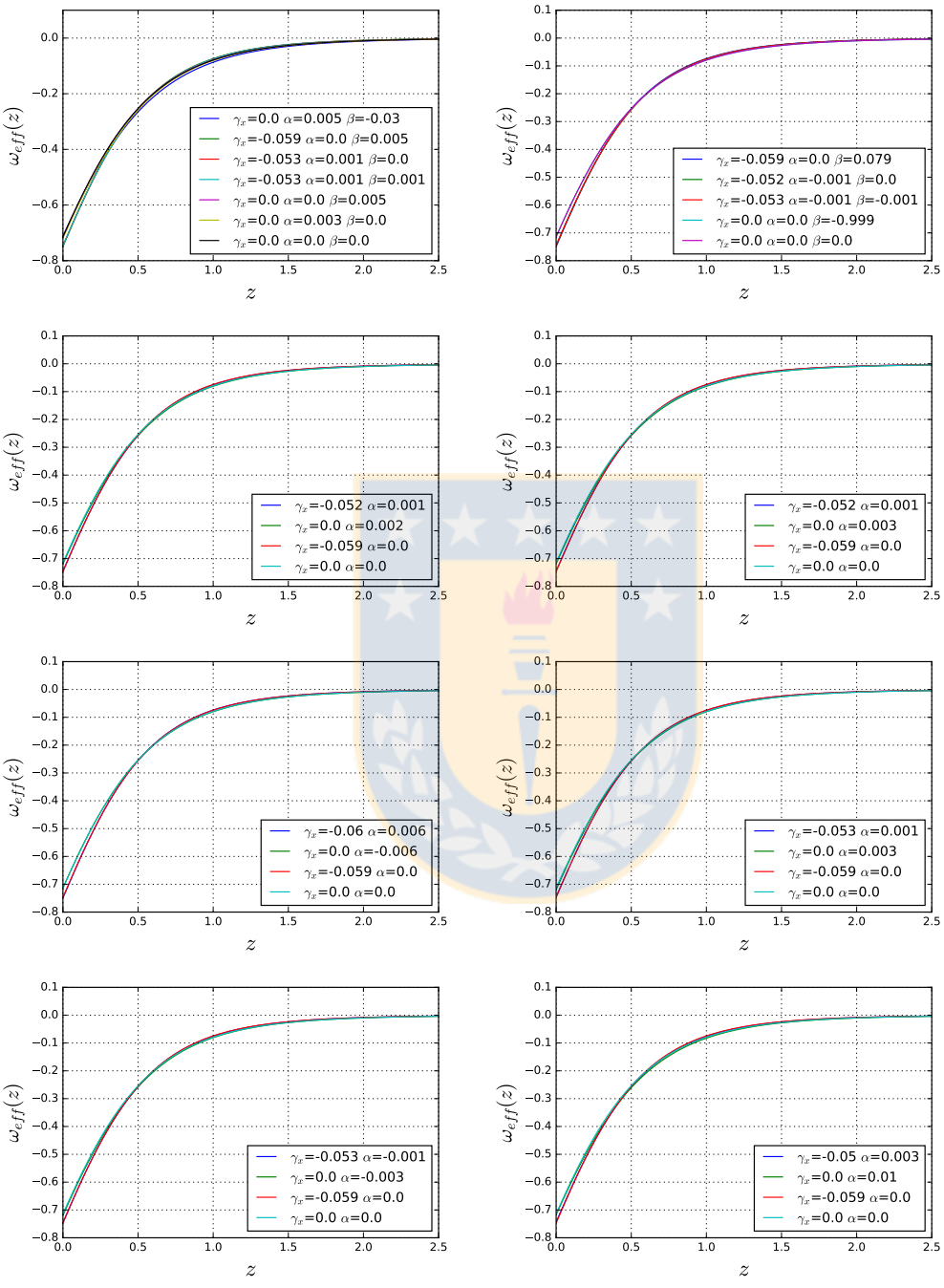

Figure 4.6: Effective parameter of state ω_{eff} considering data from Union 2.1, $H(z)$ and BAO. The graphics are ordered by the number of interaction, from Γ_1 to Γ_8, from left to right and from top to bottom. Source: Own elaboration.

Model	$\Omega_{\rm m}$	$\gamma_{\rm x}$	α	β	h	q_0	$\omega_{\rm eff}$	Age	AIC	BIC
Γ_{1d}	0.218 ± 0.073	Fixed	Fixed	0.123 ± 0.185	0.651 ± 0.005	-0.597 ± 0.110	-0.731 ± 0.073	14.065 ± 1.289	495.674	507.830
Γ_{1e}	0.229 ± 0.037	Fixed	0.124 ± 0.115	Fixed	0.652 ± 0.005	-0.581 ± 0.056	-0.721 ± 0.037	13.548 ± 1.128	495.078	507.235
Γ_{2d}	0.229 ± 0.037	Fixed	-0.11 ± 0.091	Fixed	0.652 ± 0.005	-0.581 ± 0.056	-0.721 ± 0.037	13.548 ± 1.128	495.078	507.235
Γ_{3a}	0.232 ± 0.034	Fixed	0.076 ± 0.068	$- - -$	0.651 ± 0.005	-0.576 ± 0.051	-0.717 ± 0.034	13.444 ± 1.142	495.022	507.179
Γ_{4a}	0.238 ± 0.029	Fixed	0.194 ± 0.163	$- - -$	0.651 ± 0.005	-0.568 ± 0.044	-0.712 ± 0.029	13.285 ± 1.174	494.954	507.110
Γ_{5a}	0.221 ± 0.092	Fixed	0.195 ± 0.387	$- - -$	0.651 ± 0.006	-0.593 ± 0.139	-0.729 ± 0.092	14.149 ± 1.476	495.920	508.076
Γ_{6a}	0.221 ± 0.052	Fixed	0.066 ± 0.073	$- - -$	0.652 ± 0.005	-0.593 ± 0.078	-0.729 ± 0.052	13.774 ± 1.207	495.327	507.483
Γ_{7a}	0.229 ± 0.037	Fixed	-0.124 ± 0.115	$- - -$	0.652 ± 0.005	-0.581 ± 0.056	-0.721 ± 0.037	13.548 ± 1.128	495.078	507.234
Γ_{8a}	0.252 ± 0.112	Fixed	-0.057 ± 0.484	$- - -$	0.650 ± 0.006	-0.546 ± 0.168	-0.698 ± 0.112	14.370 ± 1.470	496.270	508.426
ωCDM	0.298 ± 0.050	-0.123 ± 0.185	Fixed	$- - -$	0.651 ± 0.005	-0.597 ± 0.199	-0.731 ± 0.133	14.065 ± 0.680	495.674	507.830
ΛCDM	0.265 ± 0.021	Fixed	Fixed	$- - -$	0.649 ± 0.004	-0.526 ± 0.031	-0.684 ± 0.021	14.301 ± 0.276	494.301	502.406

Table 4.6: Results of the data fitting using the joint analysis from Constitution and $H(z)$. Source: Own elaboration.

Model	$\Omega_{\rm m}$	$\gamma_{\rm x}$	α	β	h	q_0	$\omega_{\rm eff}$	Age	AIC	BIC
Γ_{1d}	0.196 ± 0.057	Fixed	Fixed	0.078 ± 0.134	0.702 ± 0.004	-0.640 ± 0.086	-0.760 ± 0.057	13.644 ± 1.157	564.203	577.318
Γ_{1e}	0.205 ± 0.032	Fixed	0.091 ± 0.110	Fixed	0.701 ± 0.004	-0.627 ± 0.048	-0.752 ± 0.032	13.271 ± 1.081	563.949	577.063
Γ_{2d}	0.205 ± 0.032	Fixed	-0.084 ± 0.092	Fixed	0.701 ± 0.004	-0.627 ± 0.048	-0.752 ± 0.032	13.271 ± 1.081	563.949	577.063
Γ_{3a}	0.207 ± 0.029	Fixed	0.058 ± 0.068	$- - -$	0.701 ± 0.004	-0.624 ± 0.044	-0.749 ± 0.029	13.19 ± 1.110	563.931	577.046
Γ_{4a}	0.211 ± 0.025	Fixed	0.154 ± 0.174	$- - -$	0.701 ± 0.004	-0.618 ± 0.037	-0.745 ± 0.025	13.057 ± 1.168	563.912	577.027
Γ_{5a}	0.197 ± 0.070	Fixed	0.119 ± 0.253	$- - -$	0.701 ± 0.005	-0.639 ± 0.105	-0.759 ± 0.070	13.704 ± 1.292	564.324	577.439
Γ_{6a}	0.199 ± 0.044	Fixed	0.044 ± 0.061	$- - -$	0.702 ± 0.004	-0.636 ± 0.066	-0.758 ± 0.044	13.453 ± 1.129	564.064	577.179
Γ_{7a}	0.205 ± 0.032	Fixed	-0.091 ± 0.110	$- - -$	0.701 ± 0.004	-0.627 ± 0.048	-0.752 ± 0.032	13.271 ± 1.081	563.949	577.063
Γ_{8a}	0.205 ± 0.080	Fixed	-0.085 ± 0.279	$- - -$	0.701 ± 0.005	-0.627 ± 0.120	-0.752 ± 0.080	13.891 ± 1.186	564.449	577.564
ωCDM	0.252 ± 0.040	-0.078 ± 0.134	$- - -$	$- - -$	0.702 ± 0.004	-0.640 ± 0.156	-0.760 ± 0.104	13.644 ± 0.598	564.203	577.318
ΛCDM	0.229 ± 0.016	$- - -$	$- - -$	$- - -$	0.700 ± 0.003	-0.591 ± 0.024	-0.728 ± 0.016	13.825 ± 0.234	562.574	571.317

Table 4.7: Results of the data fitting using the joint analysis from Union 2 and $H(z)$. Source: Own elaboration.

and BAO and Union 2, $H(z)$ and BAO where $\gamma_{\rm x}$ is negative for all interacting models). Furthermore, as in Figure 4.1 for these data, all models have "evidence against" according to BIC compared to ΛCDM .

In Table 4.5, considering data from Union 2, $H(z)$ and BAO, we obtain that the parameter of state of DE $\gamma_{\rm x}$ for all interactions is negative (the same as Union 2.1, $H(z)$ and BAO). Furthermore, according to BIC, ΛCDM is the "best model" and the results are consistent with Table 4.1 where the interacting models with same number of free parameters are in the same region of "evidence".

The evolution of the deceleration parameter q (2.1.26) and the effective parameter of state $\omega_{\rm eff}$ (2.3.1), for the interacting models have a similar behavior compared to the ΛCDM model, see Figure 4.5 and Figure 4.6 (considering Union 2.1, $H(z)$ and BAO). The interacting models agree that the Universe is in a phase of accelerated expansion. Furthermore, according to Figure 4.6 the effective fluid in the Universe corresponds to "dark energy" because, the effective parameter of state $\omega_{\rm eff}$ for all cases take values between 0 and -1.

The graphics of q and $\omega_{\rm eff}$ for other data sets will not be shown because the results have a similar behavior to Figure 4.5 and Figure 4.6 respectively.

Comparing results of Tables 4.6, 4.7 and 4.2, where it was considered only SN Ia and $H(z)$ data sets, we noticed that all signs of the interacting term coincide in the tables. Furthermore, for these three different data sets the interacting term Γ_{8a} is negative, this means that today the energy transfer is from DM to DE. On the other hand, considering Union 2 or Union 2.1, $H(z)$ and BAO, Γ_8 and Γ_{8a} have a positive interaction, i.e., the energy transfer is from DE to DM today.

Finally, it is important to remark that all tables corresponding to different data, are consistent respect to our analysis about BIC in Table 4.1, i.e., interacting models with same number of f.p. are in the same region of "evidence". This implies that interacting models with the same number of f.p. can not be distinguish according to BIC.

Chapter 5

Conclusion

In this work we analyzed eight general types of interacting models of the dark sector with analytical solutions and compared how well they fit the joint data from Union 2.1+H(z)+BAO using the Akaike information criterion and the Bayesian information criterion. The main goal of our work was to investigate if more complex interacting models (more complex meaning models with more free parameters) are competitive in fitting the data and whether we could distinguish them via AIC and BIC. Taking into account the theoretical problems that the ΛCDM scenario presents and the observational tensions recently reported with this model [15], we assume that a departure from the simplest model is needed. We compared a plethora of interacting models among themselves and with the ωCDM scenario. In our analysis we noted a tension between the results using AIC and BIC: in some cases the AIC says that there is "evidence in favor" of some model, while BIC says that there is "evidence against" the same model. Therefore, we decided to follow the more stringent criterion, namely the BIC. According to our results, under the BIC "there is not enough evidence against" any interacting model with three free parameters when we assume that the underlying model is the one which has the lowest BIC parameter, which turns out to be ωCDM. Among the interacting models, Γ_{8a} is the model with the lowest BIC parameter value, it corresponds to a sign-changeable interaction with $\gamma_{\rm x} = 0$ and $\gamma_{\rm m} = 1$ and it is compatible with ωCDM. Furthermore, Γ_{8a} is one of the models that alleviate the coincidence problem, since the value of the coincidence parameter in the future tends to a constant (see Fig. 4.3).

Since cosmological interaction is a "phenomenological" coupling in the dark sector, i.e., there is no known physical principle that determines the interacting term, we selected the studied models under the criterion of "analytical resolution of equations", which includes many interacting models. For the selected models we concluded that all the considered models with 3 free parameters are compatible among them, i.e. all they have a BIC parameter in the same range, thus these models are not distinguishable, generating in this sense a new kind of degeneracy problem. A similar behavior appears when we inspect models with 4 free parameters as we see in Table 4.3. Furthermore, it is worth to emphasize that all the interacting models with 3 free parameters adjust the data as well as the ωCDM model.

When we compare models with 3 free parameters to models with 4 free parameters (using BIC) we find "evidence against" the 4 free parameters models when we assume that the underlying model is a 3 free parameters interacting model.

In the development of our work, we had problems to include a larger number of parameters (5 free parameters or more). When we consider 5 or more free parameters, the Python routine is not able to determine the value of the parameters in the studied ranges. In particular, when we considered the parameters of interaction α and β to be free, the confidence intervals of the parameters increases significantly, i.e., there are many values for the parameters that lead to in the same value of $\chi^2_{\rm min}$. We think that this issue can be caused by the design of the routine or because the data is not enough to determine all these parameters. In the same way, if we consider just $H(z)$ and SN Ia data, we cannot fit more than 3 free parameters, since,

it is necessary to include data from another epoch of the evolution of the Universe to fit the interaction parameters.

Finally, we conclude that an increase of the complexity of interacting models, measured through the number of free parameters, is strongly penalized according to BIC in the description of the late Universe.

In the near future we expect to be able to improve our analysis by considering different parameterizations for the DE state parameter. For this purpose first we should analyze the models through more sophisticated methods to constrain data, such as Markov Chain methods [57] to avoid problems with the increasing number of free parameters. Furthermore, in future works we expect to address the dark degeneracy problem between interacting models and parameterizations of the dark energy state parameter.

Appendix A

Elements of data fitting

A.1 Chi-Square Distribution

The Chi-Square distribution has importance in statistics and it is used in a variety situations, for example, in chi-squared tests for goodness of fit or in the confidence interval estimation. In particular this distribution will arise in the study of the variance when the underlying distribution is normal and also in goodness of fit tests. It is defined as

$$X(\chi^2, \nu) = \frac{(\chi^2)^{(\nu/2-1)} \exp[-\chi^2/2]}{2^{\nu/2}\Gamma(\nu/2)}, \tag{A.1.1}$$

where $X d\chi^2$ is the probability density of finding a value of χ^2 between χ^2 and $\chi^2 + d\chi^2$ and

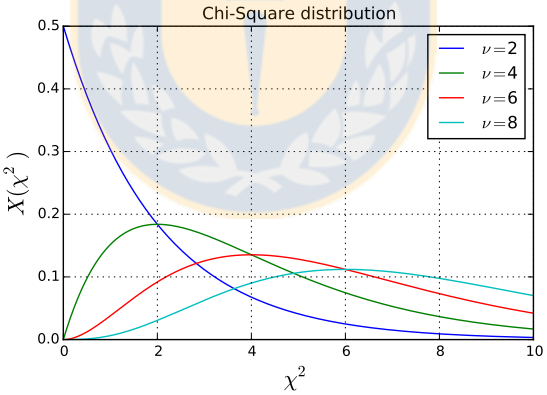

Figure A.1: Chi-square distribution for different values of ν. Source: Own elaboration.

$\nu \in \mathbb{N}$ is called "degrees of freedom". It can be shown that χ^2 has an expectation value, or mean, of ν with a standard deviation of $\sigma_{\chi^2} = \sqrt{2\nu}$ [58].

The probability of observing a value of χ^2 that is larger than a particular value χ_0^2, with ν degrees of freedom[1] is the integral of this probability

$$P(\chi_0^2 < \chi^2, \nu) = \frac{1}{2^{\nu/2}\Gamma(\nu/2)} \int_{\chi_0^2}^{\infty} (\chi^2)^{(\nu/2-1)} e^{-\chi^2/2} d(\chi^2). \tag{A.1.2}$$

[1] When fitting N independent data points with a function with L parameters the number of degrees of freedom is $\nu = N - L$.

A.2 Confidence Limits on Estimated Model Parameters

In this section, we will be more explicit regarding the precise meaning of quantitative uncertainties, and to give further information about how quantitative confidence limits on fitted parameters can be estimated. We assume that there is some underlying true set of parameters $\mathbf{a}_{\text{true}}$ that are hidden from the experimenter. These true parameters are statistically realized, along with random measurement errors, as a measured data set, which we will symbolize as $\mathcal{D}_{(0)}$. The data set $\mathcal{D}_{(0)}$ is known to the experimenter. Who fits the data to a model by χ^2 minimization or some other technique and obtains fitted values for the parameters, which we denote as $\mathbf{a}_{(0)}$.

Since measurement errors have a random component, $\mathcal{D}_{(0)}$ is not a unique realization of the true parameters $\mathbf{a}_{\text{true}}$. Moreover, there are infinitely many other possible realizations of the true parameters as "hypothetical data sets" each of which could have been the one measured. Let us denote these by $\mathcal{D}_{(1)}$,$\mathcal{D}_{(2)}$, ... Each one, had it been realized, would have given a slightly different set of fitted parameters, $\mathbf{a}_{(1)}$, $\mathbf{a}_{(2)}$, ..., respectively. These parameter sets $\mathbf{a}_{(i)}$ therefore occur with some probability distribution in the $L-$dimensional space of all possible parameter sets $\mathbf{a}_{(i)}$ (with L the number of parameters of the model). The actual measured set $\mathbf{a}_{(0)}$ is one member drawn from this distribution.

Even more interesting than the probability distribution of $\mathbf{a}_{(i)}$ would be the distribution of the difference $\mathbf{a}_{(i)}-\mathbf{a}_{\text{true}}$. This distribution differs from the former one by a translation that puts Nature's true value at the origin. If we knew *this* distribution, we would know everything that there is to know about the quantitative uncertainties in our experimental measurement $\mathbf{a}_{(0)}$. So, we need to find some way of estimating or approximating the probability distribution of $\mathbf{a}_{(i)}-\mathbf{a}_{\text{true}}$ without knowing $\mathbf{a}_{\text{true}}$ and without having available to us an infinity of hypothetical data sets.

First, we need to clarify the difference between the hypothetical data sets and the synthetic data sets. The hypothetical data sets are different realizations of the experimental data, that have certain statistic around the "true data". But the synthetic data sets are simulations of the data (using the same statistic of the hypothetical data) taking as "true data" one of the hypothetical data sets. We will denote the obtained parameters fitting the synthetic data as "$\mathbf{a}^S$".

A.3 Probability Distribution in the Normal Case

In this section we will discuss some properties of chi-square function, when the variability of data is normal distributed.

Theorems for normal distributions

Theorem A. χ^2_{min} is distributed as a chi-square distribution with $N-I$ degrees of freedom, where N is the number of data points and I is the number of fitted parameters [39].

Theorem A applies both for χ^2 with hypothetical data sets or synthetic data sets.

Theorem B. We assume that $\mathbf{a}^S_{(j)}$ is drawn from the Universe of simulated data sets with actual parameters $\mathbf{a}_{(0)}$, then the probability distribution of $\delta\mathbf{a} := \mathbf{a}^S_{(j)} - \mathbf{a}_{(0)}$ is the multivariate normal distribution

$$P(\delta\mathbf{a})da_0\ldots da_{I-1} = \text{const.}\times\exp\left(-\frac{1}{2}\delta\mathbf{a}\cdot\alpha\cdot\delta\mathbf{a}\right)da_0\ldots da_{I-1}, \tag{A.3.1}$$

where α is the inverse of the covariance matrix [39].

Theorem C. If $\mathbf{a}^S_{(j)}$ is drawn from the Universe of simulated data sets with actual parameters $\mathbf{a}_{(0)}$, then the quantity $\Delta\chi^2 := \chi^2(\mathbf{a}_{(j)})-\chi^2(\mathbf{a}_{(0)})$ is distributed as a chi-square distribution with I degrees of freedom (here the χ^2's are all evaluated using the fixed (actual) data set $\mathcal{D}_{(0)}$) [39].

Theorem D. Assume that $\mathbf{a}_{(j)}^{S}$ is drawn from the Universe of simulated data sets, that its first ν components $a_0, a_1, ...a_{\nu-1}$ are held fixed, and that its remaining $I - \nu$ components are varied so as to minimize χ^2. We call this minimum value χ^2_ν. Then $\Delta\chi^2_\nu := \chi^2_\nu - \chi^2_{\min}$ is distributed as a chi-square distribution with ν degrees of freedom, where $\chi^2_{\min}$ is obtained without fixing any parameter.

Let $\delta\mathbf{a}$ be a change in the parameters whose first component is arbitrary, δa_0, but the rest of whose components are chosen to minimize the $\Delta\chi^2$. Then Theorem D applies and the value of $\Delta\chi^2$ is given in general by

$$\Delta\chi^2 = \delta\mathbf{a} \cdot \alpha \cdot \delta\mathbf{a}. \tag{A.3.2}$$

Otherwise, it is possible to demonstrate that in general

$$\delta a_i = \pm\sqrt{\Delta\chi^2_\nu}\sqrt{C_{ii}}, \tag{A.3.3}$$

with C the covariance matrix.

p	ν		
	1	2	3
68.27%	1.00	2.30	3.53
90%	2.71	4.61	6.25
95.45%	4.00	6.18	8.02
99%	6.63	9.21	11.3

Table A.1: $\Delta\chi^2$ as a function of confidence level p and number of parameters ν. Source: Own elaboration.

In the Fig. A.2 we can see two examples of table A.1

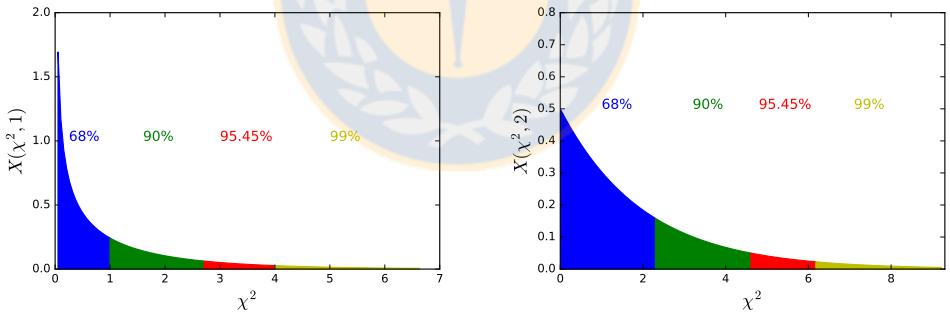

Figure A.2: χ^2 distribution for $\nu = 1$ (left) and $\nu = 2$ (right). Source: Own elaboration.

On the other hand, we can plot contours of χ^2 to see the enclosed region for different values of $\Delta\chi^2$. A contour line of a function of two variables is a curve along which the function has a constant value (a function of three variables define a contour surface). It is a cross-section of the three-dimensional graph of the function $f(x, y)$ parallel to the xy plane.

Example 1: Straight line

Suppose we want to study a physical phenomenon with equation $y = 2x$ and we have a linear model $y = a_0 + a_1 x$. Then, the true parameters are $a_0 = 0$ and $a_1 = 2$ (remember that the parameter values are unknown for us). Since we assume random error, in our measurements, we will get other values for the parameters a_0 and a_1 (blue dots in Fig. A.3).

Rather than present all details of the probability distribution of errors in parameter estimation, it is common practice to summarize the distribution in the form of confidence limits. The

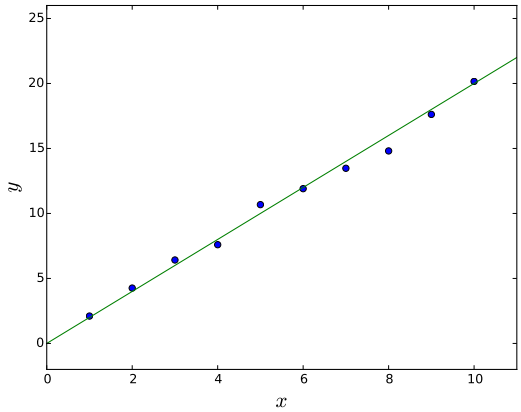

Figure A.3: Straight line example. Blue dots are the measurements (simulated using a gaussian random variability with standard deviation $\sigma_i = 0.1x_i$) and the straight line is the function $y = 2x$ from which the data points are simulated. Source: Own elaboration.

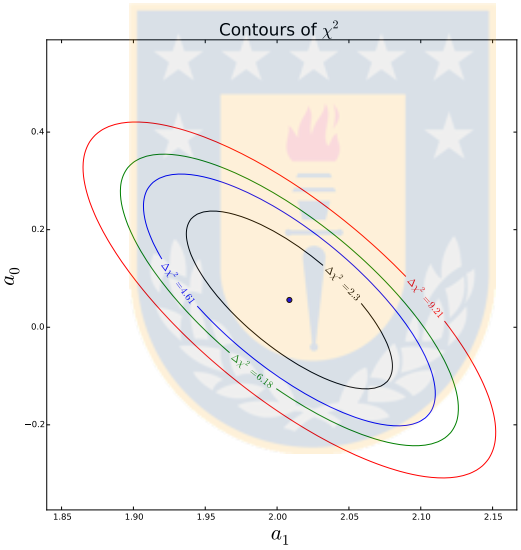

Figure A.4: These are the contours of our example. The central point corresponds to the minimum value of χ^2. Source: Own elaboration.

full probability distribution is a function defined on the I-dimensional space of parameters $\mathbf{a}$. A confidence region (or confidence interval) is just a region of that I-dimensional space (hopefully a small region) that contains a certain (large) percentage of the total probability distribution.

The only requirement is that the region does include the stated percentage of probability. Certain percentages are, however, customary in scientific usage: 68.3% (the lowest confidence worthy of quoting), 90%, 95.4%, 99%, and 99.73%. As for shape, we want a region that is compact and reasonably centred on your measurement $\mathbf{a}_{(0)}$, since the whole purpose of a confidence limit is to inspire confidence in that measured value. In one dimension, the convention is to use a line segment centred on the measured value; in higher dimensions, ellipses or ellipsoids are most frequently used.

We can use (A.3.2) to plot certain confidence regions making equal $\Delta\chi^2$ to the respective

value in table A.1.

On the other hand, we can compare Fig A.4 with a simulation of the data sets (synthetic data) and corroborate that the probability regions are the same.

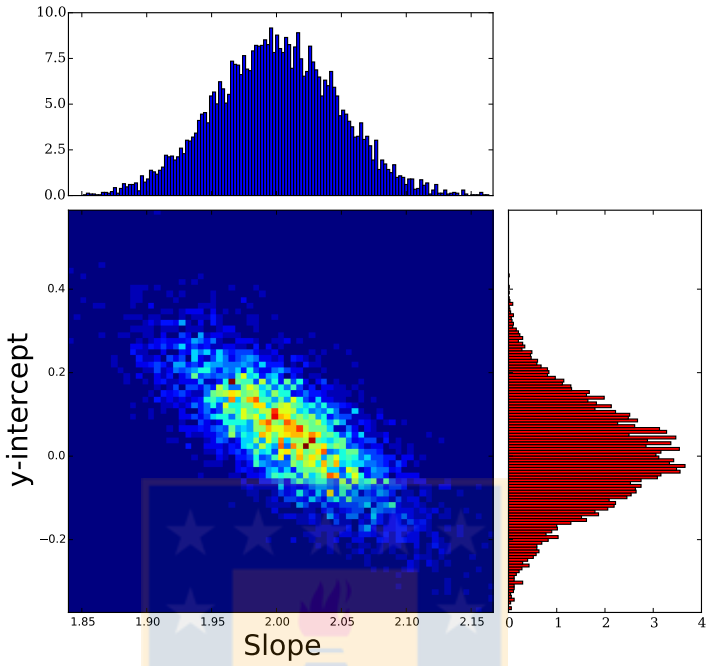

Figure A.5: Combined histograms of synthetic data. Source: Own elaboration.

Example 2: Theorems A, B, C and D

As already mentioned in the example of the straight line we have a data set with random normal errors ($\sigma_i = 0.1x_i$) and we can verify these theorems using a Monte Carlo method. We simulated 5000 data sets (ten points per set) using

$$y_i = 2x_i + \text{Normal error}. \tag{A.3.4}$$

The histogram of Fig. A.6 is composed of the different values of χ^2_{min} in each simulation.

In the case of Theorem B we will consider in the example that the first simulation is a "real data set" $\mathcal{D}_{(0)}$ and with this data set we obtained the parameters $\mathbf{a}_{(0)}$ as the best fit, then we can simulate data sets around $y(x, \mathbf{a}_{(0)})$ (synthetic data sets) with the same probability distribution as the "original data set" and compare the histogram of $\delta\mathbf{a}$ with the equation (A.3.1).

Theorem C is very important since it makes the connection between particular values of $\Delta\chi^2$ and the fraction of the probability distribution that they enclose as an I-dimensional region, i.e., the confidence level of the I-dimensional confidence region (with I the number of parameters). In our example $I = 2$ so that, we need to compare the chi-square distribution (A.1.1) (with $\nu = 2$) with the histogram of the χ^2_{min} of the synthetic data.

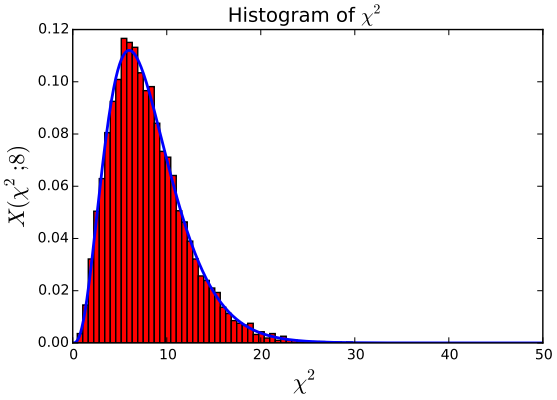

Figure A.6: Chi-square distribution of the example. We use 10 data points and 2 free parameters thus, $\nu = 8$. Source: Own elaboration.

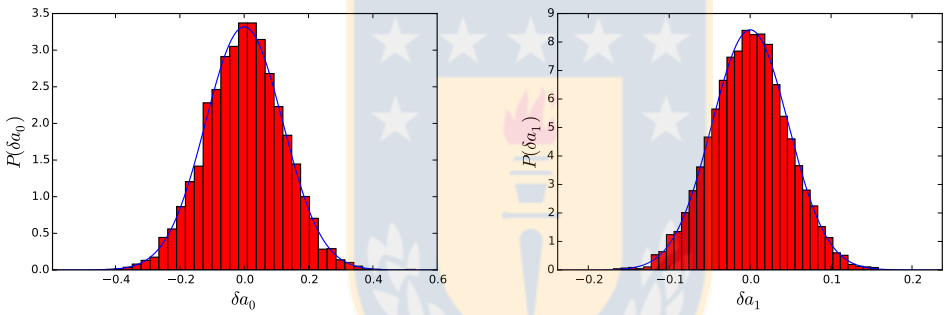

Figure A.7: Histograms of δa_0 and δa_1. To the left is the histogram of δa_0 and to the right the histogram of δa_1. Remember that, in order to see the PDF of one parameter we need to integrate over all the others parameters. Source: Own elaboration.

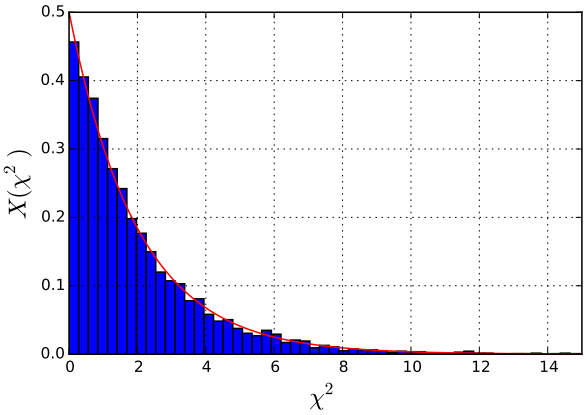

Figure A.8: Histogram of $\Delta\chi^2$. Source: Own elaboration.

To test Theorem D we have fixed the parameter a_0 and we simulate again data sets, but in this case we can only fit a_1 to the data sets. Since now we have two parameters and we have fixed one, we will have $\nu = 1$ for the chi-square distribution.

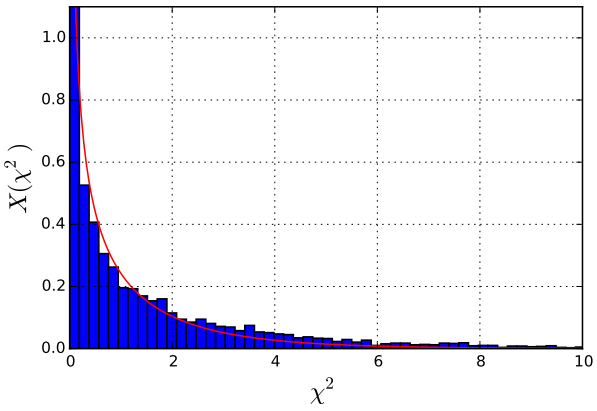

Figure A.9: Histogram of $\Delta\chi^2_\nu$, where a_0 was set and a_1 was fitted in each simulation. Source: Own elaboration.

A.3.1 Example 3: Maximum Likelihood

In our case $f(x_i) = a_1 x_i + a_0$ and if the data has random error with normal distribution, then

$$P_i \propto e^{-\frac{(f(x_i)-y_i)^2}{\sigma_i^2}}, \tag{A.3.5}$$

with σ_i the standard deviation of the random error. Then, the likelihood function will be

$$\mathcal{L} \propto \prod_{i=0}^{N} e^{-\frac{(a_0+a_1x_i-y_i)^2}{\sigma_i^2}}, \tag{A.3.6}$$

and finally $\mathcal{M} = \ln \mathcal{L}$ will be given by

$$\mathcal{M} \propto \sum_{i=1}^{M} \frac{(a_1x_i + a_0 - y_i)^2}{\sigma_i^2} + D, \tag{A.3.7}$$

where D is a normalization constant that we omit from here on. It can be seen, when data has a normal variability, the maximum likelihood method reduces to the method of minimum squares.

A.4 Propagation of uncertainties

Let $f(\mathbf{a})$ a function of the parameters $a_0, a_1, \ldots, a_n$, and σ_l the variance of the l-th parameter. Then, neglecting correlations or assuming independent variables yields a common formula to calculate error propagation

$$\Sigma = \sqrt{\left(\frac{\partial f}{\partial a_0}\right)^2 \sigma_0^2 + \left(\frac{\partial f}{\partial a_1}\right)^2 \sigma_1^2 + \cdots + \left(\frac{\partial f}{\partial a_n}\right)^2 \sigma_n^2}, \tag{A.4.1}$$

where Σ represents the standard deviation of the function f, σ_i represents the standard deviation of the a_i parameter.

A.5 Minimization Algorithm

To minimize the Chi-Squared function we utilize a python software routine. Specifically, we use the lmfit package that it is designed to provide simple tools to help you build complex fitting models for non-linear least-squares problems and apply these models to real data. This package has different minimization algorithms as for example Levenberg-Marquardt, Nelder-Mead, L-BFGS-B, Powell, Conjugate Gradient, Newton-CG and so on. In particular we use use the least-squares method based in the Levenberg-Marquardt algorithm, also known as Damped least-squares (DLS) method. The DLS is used for solving generic curve-fitting problems. However, as for many fitting algorithms, the DLS finds only a local minimum, which is not necessary the global minimum. The DLS can finds in many cases a solution even if it starts very far off the final minimum.

Remembering (3.2.2) we have that

$$\chi^2(\mathbf{a}) = \sum_{i=0}^{N-1} \left[\frac{y_i - f(x_i, \mathbf{a})}{\sigma_i} \right]^2. \tag{A.5.1}$$

Like other numeric minimization algorithms, the Levenberg-Marquardt algorithm is an iterative procedure. To start a minimization, the user has to provide an initial guess for the parameter vector, $\mathbf{a}$. In each iteration step, the parameter vector $\mathbf{a}$, is replaced by a new estimate, $\mathbf{a} + \delta$.

For simplicity rewrite (A.5.1) as

$$\chi^2(\mathbf{a}) = \sum_{i=0}^{N-1} |K_i(\mathbf{a})|^2 = K^T(\mathbf{a}) K(\mathbf{a}), \tag{A.5.2}$$

where

$$K_i(\mathbf{a}) = \frac{y_i - f(x_i, \mathbf{a})}{\sigma_i} \tag{A.5.3}$$

To determine $\boldsymbol{\delta}$, the functions $K(x_i, \mathbf{a} + \boldsymbol{\delta})$ are approximated by their linearizations

$$K(\mathbf{a} + \boldsymbol{\delta}) \approx K(\mathbf{a}) + J\boldsymbol{\delta}, \tag{A.5.4}$$

where

$$J_i = \frac{\partial f(x_i, \mathbf{a})}{\partial \mathbf{a}}, \tag{A.5.5}$$

with this notation the gradient of χ^2 is

$$\nabla\chi^2(\mathbf{a}) = 2J^T(\mathbf{a}) K(\mathbf{a}). \tag{A.5.6}$$

We want to minimize the χ^2 and this occur when the gradient of $\chi^2(\mathbf{a} + \boldsymbol{\delta})$ goes to zero then,

$$\begin{aligned} \nabla\chi^2(\mathbf{a} + \boldsymbol{\delta}) &= 2J^T(\mathbf{a} + \boldsymbol{\delta}) K(\mathbf{a} + \boldsymbol{\delta}) && \text{(A.5.7)} \\ &= 2J^T(\mathbf{a} + \boldsymbol{\delta})[K(\mathbf{a}) + J(\mathbf{a})\boldsymbol{\delta}] && \text{(A.5.8)} \\ &\approx 2J^T(\mathbf{a})[K(\mathbf{a}) + J(\mathbf{a})\boldsymbol{\delta}] = 0, && \text{(A.5.9)} \end{aligned}$$

then, we need to solve

$$\boldsymbol{\delta} = -\left[J^T(\mathbf{a}) J(\mathbf{a})\right]^{-1} J^T(\mathbf{a}) K(\mathbf{a}). \tag{A.5.10}$$

Of this form to find the minimum of χ^2 in each iteration we need to search in the direction $\mathbf{a}_{k+1} = \mathbf{a}_k + \alpha\boldsymbol{\delta}$, with α a dimensionless parameter. The iteration stops when

$$|\mathbf{a}_{k+1} - \mathbf{a}_k| < \mathbf{a}_{\text{tol}}, \tag{A.5.11}$$

and

$$|\chi^2_{k+1} - \chi^2_k| < \chi^2_{\text{tol}}, \tag{A.5.12}$$

where $\mathbf{a}_{\text{tol}}$ and χ^2_{tol} are the relative tolerances of the error desired in the sum of squares. Deriving two times (A.5.1) and despising terms with second derivatives (since they may present numerical problems) is easy to show that the covariance matrix is written as

$$\text{Cov} = [J^T J]^{-1}. \tag{A.5.13}$$

This is the algorithm that we use to minimize the χ^2 function, and it is implemented in python in the function leastsq from the scipy package. By default the leastsq function has a relative tolerance for $\mathbf{a}_{\text{tol}}$ and χ^2_{tol} of 1.49012×10^{-8}. The assigned errors to the estimation parameters are calculated using (A.5.13).

Bibliography

[1] Steven Weinberg *Cosmology*, Oxford (2008).

[2] E. J. Copeland, M. Sami and S. Tsujikawa, Int. J. Mod. Phys. D **15**, 1753 (2006).

[3] P. A. R. Ade *et al.* [Planck Collaboration], Astron. Astrophys. **594**, A13 (2016).

[4] R. G. Riess *et al.*, Astrophys. J. **826**, no. 1, 56 (2016) ; A.G. Riess et al., Astrophys. J. 730, 119 (2011). Erratum: [Astrophys. J. 732, 129 (2011)].

[5] J. Magaña, V. H. Cárdenas and V. Motta, JCAP **1410**, 10, 017 (2014).

[6] B. Ratra, P. J. E. Peebles, Phys. Rev. D, 37, 3406 (1988).

[7] W. Zimdahl, D. Pavon and L. Chimento, Phys. Lett. B **521**, 133 (2001).

[8] A. Nunes, J. P. Mimoso and T. C. Charters, Phys. Rev. D **63**, 083506 (2001).

[9] G. Mangano, G. Miele and V. Pettorino, Mod. Phys. Lett. A **18**, 831 (2003).

[10] W. Zimdahl, D. Pavón, L. Chimento, A. S. Jakubi, astro-ph/0404122.

[11] R. Curbelo, T. Gonzalez, G. Leon and I. Quiros, Class. Quant. Grav. **23**, 1585 (2006).

[12] R. G. Cai and Q. Su, Phys. Rev. D **81**, 103514 (2010).

[13] A. Kurek, M. Szydlowski, A. Krawiec, M. Kamionka, *Eur. Phys. Journal*, 1-12 (2014).

[14] F. E. M. Costa and J. S. Alcaniz,Phys. Rev. D **81**, 043506 (2010); F. E. M. Costa, E. M. Barboza, Jr. and J. S. Alcaniz, Phys. Rev. D **79**, 127302 (2009); J. F. Jesus, R. C. Santos, J. S. Alcaniz and J. A. S. Lima, Phys. Rev. D **78**, 063514 (2008); Q. Wu, Y. Gong, A. Wang and J. S. Alcaniz, Phys. Lett. B **659**, 34 (2008).

[15] R. Murgia, S. Gariazzo and N. Fornengo, JCAP **1604**, no. 04, 014 (2016).

[16] H- Wei. Commun. Theor. Phys. **56**, 972 (2011).

[17] B. Wang, E. Abdalla, F. Atrio-Barandela and D. Pavón, Rept. Prog. Phys. **79**, no. 9, 096901 (2016).

[18] Luis P. Chimento, Phys. Rev. D **81**, 043525 (2010).

[19] M. Kunz, Phys. Rev. D **80**, 123001 (2009).

[20] S. Carneiro and H. A. Borges, JCAP **1406**, 010 (2014); H. Velten, H. A. Borges and T. R. P. Carames, Phys. Rev. D **93**, no. 6, 063503 (2016).

[21] Luis P. Chimento, AIP Conf. Proc., **1471** 30-38 (2012)

[22] E. Hubble, *Proc. N.A.S.* **15** 168-173 (1929)

[23] A. A. Penzias y R. W. Wilson, Astrophysical Journal **142**, 419 (1965)

[24] A.G. Riess, et al., Astron.J. **116** (1998)

[25] S. Perlmutter *et al.* [Supernova Cosmology Project Collaboration], Astrophys. J. **517**, 565 (1999).

[26] M. Betoule *et al.* [SDSS Collaboration], Astron. Astrophys. **568**, A22 (2014).

[27] Scott Dodelson, *Modern Cosmology*, Academic Press (2011).

[28] E. J. Copeland, M. Sami and S. Tsujikawa, Int. J. Mod. Phys. D **15**, 1753 (2006).

[29] Supernova Cosmology project, http://supernova.lbl.gov/union/.

[30] M. Hicken et al., Astrophysical Journal **700**, Issue 2, pp. 1097-1140 (2009).

[31] Liao, K., Li, Z., Ming, J., Zhu, Z.-H., Physics Letters B, 718, 1166 (2013).

[32] D. J. Eisenstein, *et al.* [SDSS Collaboration], Astrophys. J. **633**, 560 (2005).

[33] Alcock C., Paczynski B., 1979, Nat, 281, 35.

[34] G. Hinshaw , The Astrophysical Journal Supplement Series, 208, 2, 19 (2013).

[35] L. Page et al. [WMAP Collaboration], Astrophys. J. Suppl. **148**, 233 (2003).

[36] W. Hu and N. Sugiyama, Astrophys. J. **471**, 542 (1996).

[37] J. R. Bond, G. Efstathiou and M. Tegmark, Mon. Not. Roy. Astron. Soc. **291**, L33 (1997).

[38] Richard Feynman, *Lectures of Physics*, **1**, 1 (1963).

[39] William H. Press, Saul A. Teukolsky, William T. Vetterling, Brian P. Flannery, *Numerical Recipes*, Cambridge (2007).

[40] A. Kurek, M. Szydlowski, *Astrophys Journal*, 1-7 (2008).

[41] R. Trotta, Contemp. Phys. **49**, 71 (2008).

[42] A. R. Liddle, Ann. Rev. Nucl. Part. Sci. **59**, 95 (2009).

[43] Akaike, Hirotugu, IEEE Transactions on Automatic Control 19 (6): 716-723 (1974).

[44] Schwarz, Gideon E., Annals of Statistics, 6 (2) 461-464 (1978).

[45] A. R. Liddle, Mon. Not. Roy. Astron. Soc. **351**, L49 (2004).

[46] W. Godlowski and M. Szydlowski, Phys. Lett. B **623**, 10 (2005).

[47] D. R. Castro, H. Velten and W. Zimdahl, JCAP **1206**, 024 (2012).

[48] Kullback, S. Leibler, R.A., Annals of Mathematical Statistics **22 (1)** 79-86, (1951).

[49] Jeffreys, H., *Theory of Probability*, Oxford Univ. Press.

[50] Robert E. Kass, Adrian E. Raftery, Journal of the American Statistical Association, Vol. 90, No. 430, 773-795 (1995).

[51] G. Mangano, G. Miele, S. Pastor, T. Pinto, O. Pisanti and P. D. Serpico, Nucl. Phys. B **729**, 221 (2005).

[52] Liao, K., Li, Z., Ming, J., Zhu, Z.-H., Physics Letters B, **718**, 1166 (2013).

[53] Blake C. *et al.*, MNRAS, 1598 (2011).

[54] Percival W. J. *et al.*, MNRAS, **401**, 2148 (2010).

[55] Beutler F. et al., MNRAS, **416**, 3017, (2011).

[56] F. Arevalo, P. Cifuentes, S. Lepe and F. Pena, Astrophys. Space Sci. **352**, 899 (2014).

[57] J. Akeret, S. Seehars, A. Amara, A. Refregier, A. Csillaghy, Astronomy and Computing, **2**, 27-39 (2013).

[58] Ifan G. Hughes, Thomas P. A. Hase, *Measurements and their Uncertainties*, Oxford (2010).

[59] R. Lazkoz, S. Nesseris and L. Perivolaropoulos, JCAP **0511** (2005).

[60] Edmund J. Copeland, M. Sami, Shinji Tsujikawa, *International Journal of Modern Physics*, 1-93 (2006).